ISSN 0252-1075
Contribution from IITM
Research Report No. RR-099

Measurement of Profiles and Surface Energy Fluxes On the West Coast of India at Vasco-Da-Gama, Goa During ARMEX 2002-03

S. Sivaramakrishnan, B.S. Murthy, T. Dharmaraj,
Cini Sukumaran and T. Rajitha Madhu Priya

August 2003

Indian Institute of Tropical Meteorology
Pune - 411 008, India

ISSN 0252-1075
Contribution from IITM
Research Report No. RR-099

Measurement of Profiles and Surface Energy Fluxes on the West Coast of India at Vasco-Da-Gama, Goa during ARMEX 2002-03

S. Sivaramakrishnan, B.S. Murthy, T. Dharmaraj, Cini Sukumaran
and
T. Rajitha Madhu Priya

August 2003

Indian Institute of Tropical Meteorology
Dr. Homi Bhabha Road, Pashan Pune - 411 008
Maharashtra, India

E-mail : lip@tropmet.ernet.in
Web : http://www.tropmet.ernet.in
Fax : 91-020-5893825
Telephone : 91-020-5893600

Contents

	Abstract	1
1.	Introduction	2
2.	Topography	2
3.	Expected features	3
4.	Experimental setup	3
5.	Data	3
6.	Results	4
6.1.	Internal Boundary Layer	4
6.2.	Characteristics of IBL at Vasco-Da-Gama site	5
6.3.	Turbulence observations	6
6.3.1.	Sonic anemometer	6
6.3.2.	H_2O/CO_2 Gas Analyzer	8
6.4.	Slow/Conventional Sensors	9
7.	Conclusions	9
8.	References	11
	Appendix A	12
	Appendix B	14
	Figures 1-16	15-30

Measurement of Profiles and Surface Energy Fluxes on the West Coast of India at Vasco-Da-Gama, Goa during ARMEX 2002-03

S.Sivaramakrishnan, B.S.Murthy, T.Dharmaraj, Cini Sukumaran and T. Rajitha Madhu Priya

Indian Institute of Tropical Meteorology, Pune 411 008, India

Abstract

As part of the Arabian Sea Monsoon Experiment (ARMEX), measurements of profiles of wind, temperature and humidity along with solar radiation and surface fluxes have been made at Vasco-Da-Gama (15°21' N, 73°51' E), Goa on the west coast of India using 9 m high meteorological tower, installed at ~ 25-30 m away from the coast in the premises of National Center for Antarctic and Ocean Research (NCAOR). The Phase I of ARMEX during June 15 – August 15, 2002, is aimed at understanding better the role of air-sea interaction and coastal atmospheric boundary layer (ABL) during the onset/active phase of the Indian summer monsoon that causes heavy precipitation on the west coast. In this report the data collected during the field campaign have been validated to ensure quality. Characteristics of the profiles and surface fluxes measured at the site during the monsoon are presented. The Internal Boundary Layer (IBL) developing very close to the coast at the site has been found to be ~ 4 m using profiles of wind and temperature. Turbulence statistics are observed to follow Monin-Obukhov universal similarity relations. Spectral analysis of the data shows peaks at scales from a few seconds to minutes during unstable conditions for water vapor and vertical velocity. The influence of precipitation on the structure of the atmospheric surface layer is described.

1. Introduction

The coastal atmospheric boundary layer is inherently heterogeneous, dominated by variations in topography, large temperature gradients and large changes in roughness. The coastal ocean is characterized by large variations in sea surface temperature and roughness and a non-equilibrium sea state. These conditions produce interactions between sea-breezes, meso-scale eddies and terrain-generated winds that cause complex flow patterns (Stull, 1988). A national field experiment, *'Arabian Sea Monsoon Experiment 2002-03 (ARMEX)'* has been evolved and implemented to collect meteorological and oceanographic data in the Arabian Sea and the West coast of India. This experiment is sponsored by the department of Science & Technology, Government of India. A number of institutions viz., Indian Institute of Tropical Meteorology, Indian Institute of Science, National Institute of Oceanography, India Meteorological Department, National Institute of Ocean Technology, etc. and some universities have participated in the field experiment. The objective of ARMEX is to understand better the role of air-sea interaction and coastal ABL in bringing heavy precipitation at some stations between 15^{o} – 16^{o} latitude on the west coast of India during the onset/active phase of the southwest monsoon. Statistical analysis of the meteorological data indicated that most of the time these heavy precipitation events were due to deep convection in the Arabian sea near the coast (~100-200 km). At times offshore trough and mid-tropospheric cyclone played an important role (*ARMEX, Science plan*). To understand in detail the deep convection, offshore trough and mid-troposphere cyclone over the Arabian sea, measurements of air-sea fluxes, vertical profiles of wind, temperature, humidity were made onboard the research vessel ORV Sagarkanya during her monsoon cruises (ARMEX, *Science Plan*) in the Arabian sea. Phase I of ARMEX during June 15 – August 15, 2002 is named '*Offshore trough*'. In addition to air-sea measurements off the west coast, some coastal stations within 15^{o} – 16^{o} latitudes representing intense rainfall on the west coast have also been identified to make measurements of surface energy fluxes. One of the stations is Vasco-Da-Gama ($15^{o}21'$ N, $73^{o}51'$ E) where a meteorological tower of 9 m height was installed to measure wind speed, direction, temperature and humidity at 1, 2, 5 and 8 m above surface. Surface fluxes of momentum, sensible heat, latent heat and carbon dioxide were measured directly following eddy correlation technique (*Appendix A* for details of sensors, range, etc.). In this report we present the surface layer profiles and flux measurements at Vasco-Da-Gama and describe their relevance to meso-scale circulation of maritime air over the station.

2. Topography

1. The 9 m high tower was installed in the campus of National Center for Antarctic and Ocean Research (NCAOR), Headland Sada, Vasco. The Headland is ~ 58.5 m AMSL.
2. The tower is located at the Arabian Sea coast at a height of ~ 35 m above sea surface at the coast and ~ 25-30 m away from the coast (**Figure 1**).
3. The NCAOR buildings are on the north about 100-150 m away from the tower.
4. The terrain surrounding the tower except on the South, consists mainly grass (~ 1 m tall), wild plants and bushes during the phase I of ARMEX.
5. The experimental site has a large fetch (Sea) in the upwind SW direction.

3. Expected features

Since the tower is just on the coast, the measurements could be very much influenced by the upwind flow from the sea (winds are SW to W) as well as the local surface conditions. Since there is a step change in surface roughness and surface temperature as the wind flows from the sea to the land, an internal/thermal boundary layer develops at the boundary between land and sea and its depth increases inland. The foot print of the measurement at 5-8 m on the tower reflects mainly maritime air characteristics in the upwind S-W quadrant. Since the tower is located very close to the coast line, the height of the internal boundary layer, IBL (a function of fetch, temperature and roughness gradient between land and sea) may be just a few meters above surface and some levels of measurement on the tower may lie within IBL. Thus measurements within the IBL reflect the properties of the local surface where as those above IBL, mainly the upwind flow (marine air) characteristics. Ambient synoptic/monsoon flow, if strong enough, may totally prevail upon the geographically generated local circulations like IBL due to small-scale irregularities at the surface.

4. Experimental set up

The schematic diagram of the experimental setup of the 9 m high tower is shown in **Figure 2**. The instruments to measure wind speed, direction, air temperature and relative humidity are located at about 1.5 m away from the tower on cross booms of 2 m length at four levels viz., 1, 2, 5 and 8 m above surface. The details of sensors/instruments are given in ***Appendix A***. Turbulence measurements were made using sonic anemometer at 5 m level and H_2O/CO_2 gas analyzer (Licor-7500 Hygrometer) at the same level with a sampling frequency of 10 Hz. In order to have contribution from all significant eddies and also keeping in view the terrain at the site, the 5 m level (instead of logarithmic level at 4 m) is chosen for direct flux and profile measurement. The 8 m level is not chosen due to operational inconvenience and risk involved during installation of expensive instruments. Solar radiation (Short wave-incoming, Short wave-outgoing, Long wave-incoming, Long wave-outgoing) were measured using Eppley radiometers only at 2 m above surface. Atmospheric pressure and rainfall were also measured by standard barometer and rain gauge respectively. Gill propeller anemometer was mounted at 5 m level to measure the three wind components at 10 Hz. The data from the slow sensors viz., cup anemometer, temperature, humidity, rainfall sensors, atmospheric pressure, solar radiation instruments, were logged into a data logger, mounted at the foot of the tower. The data from sonic anemometer, IR Hygrometer and Gill propeller anemometer were logged directly into separate personal computers, housed in a container near by the tower. Slow sensors were sampled at 1 Hz. However, only 1 minute mean values are logged.

5. Data

The 1 minute mean data from the slow sensors were checked to detect spikes due to some transient errors and were replaced with an average of preceding/succeeding values. Calibration curves, obtained earlier before the start of the experiment, were used for correction. Cup anemometers and Gill propeller anemometer were calibrated in IMD's wind tunnel. Temperature sensors were calibrated at IMD with help of a thermostat.

Humidity sensors were calibrated earlier in laboratory at IITM. Temperature and wind speed (Gill propeller anemometer) calibration curves are given in ***Appendix B***. Half an hour means were calculated from the corrected data and used to study the characteristic diurnal variation as well as variation with height of wind speed, temperature and humidity. The millivolt output from radiation sensors were converted to wm^{-2} using conversion factors, provided by the manufacturers. Weather conditions and Psychrometer observations of temperature and humidity were maintained in a log book.

6. Results

Profiles of mean wind, temperature and humidity in the atmospheric surface layer are used to study the characteristics of internal/thermal internal boundary layer very close to the sea coast. Turbulence observations by sonic anemometer and Infrared hygrometer (H_2O/CO_2 Open Path Gas Analyzer) are used to estimate surface fluxes of momentum, sensible and latent heat. CO_2 flux is also estimated using observations of CO_2 concentration density from IR hygrometer and vertical wind from Gill propeller anemometer by eddy correlation technique.

6.1 Internal boundary layer

As air passes from sea to land with different surface characteristics, it must adjust to the prevailing conditions at the boundary. The layer of air whose properties have been affected by the new surface properties is referred to as an internal boundary layer (IBL). Studies elsewhere revealed that the thickness of IBL grows with increasing distance, or fetch, downwind from the line of discontinuity, and the thickening rate depends on the relative change of roughness between the two surfaces and on the atmospheric stability. For neutral small-scale flow over a roughness change, the IBL is the layer within which significant changes from upstream conditions occur, in wind and stress (momentum flux) profiles. Discontinuities in wind profile or wind-profile 'kinks', allow its top to be identified (Garratt, 1990). Within the IBL there exists an equilibrium layer, defined in terms of 90% level of adjustment in the stress (or other vertical flux in non-neutral case).

The IBL depth (only roughness change) is parameterized as a power of the fetch (Panofsky, et.al, 1982; Smedman-Hogstrom and Hogstrom, 1978; Rao, et.al, 1974):

$$[\delta / z_{o1}] = a\ [x / z_{o1}]^{b} \qquad (1)$$

where z_{o1} is the aerodynamic roughness length upwind of the border and x is the fetch. The power, b is equal to about 0.8 for statically neutral, slightly smaller (0.6 to 0.7) in stable and larger for unstable (0.8 to 1.0) conditions. Parameter a_{IBL} is in the range of 0.2 to 0.8, being large for unstable conditions and small for stable ones. 'a' is parameterized as a function of roughness:

$$a = 0.75 + 0.03 * \ln (z_{o2} / z_{o1}) \qquad (2)$$

zo1 is as defined above and z_{o2} is the aerodynamic roughness length downwind over land. In the case of a flow from smooth to rough surface, say from sea to land, at small fetch, a

shallow layer "*feels*" the increased roughness. At greater distances, deeper layers feel the increased roughness. Above the top of IBL, i.e., above the kink in the wind profile, the wind maintains a profile characteristic of the upwind roughness (Beljaars, 1987).

In coastal regions there exists a step change in surface temperature in addition to roughness change. The IBL that develops due to land-sea temperature (surface heat flux) contrast is called thermal internal boundary layer (TIBL). Its growth rate with fetch in the downwind direction is very important for modeling the diffusion of pollutants in the coastal regions. In convective conditions in the coastal region, TIBL top is readily identified where potential temperature profile has a discontinuity (Raynor et al., 1975) or at the top of a well-mixed layer (Venkatram, 1977). In Raynor et al. (1975, 1979)'s study observed heights of TIBL (h) were found to agree with an empirical model derived from physical and dimensional reasoning, viz.,

$$h^2 = C_D \gamma^{-1} (\theta_l - \theta_s) x \qquad (3)$$

where C_D is a low-level drag coefficient over land (in the downstream direction), γ is lapse rate above the IBL and $(\theta_l - \theta_s)$ is the potential temperature difference between the land surface and the sea and x is fetch. The above equation was simplified by Hsu (1986) who found several sets of data satisfying $h = 1.9\ x^{1/2}$, with h and x in meters. For stable conditions, covering a fetch range from 5 to 500 km, Hsu arrived at $h = 0.57\ x^{1/2}$. Thus h increases with greater land roughness and greater temperature difference, and decreases with greater stability above the IBL, for a given fetch x.

6.2 Characteristics of IBL at Vasco-Da-Gama site

The frequency distribution of wind direction at 5 m above surface (from sonic anemometer) shows that 45% of the time during the period 13-28 July, it blows from 260-280 degrees i.e., WSW-W direction (**Figure 3**). Most of the time winds are about 5 – 6 ms^{-1}. Analysis of wind and direction data from cup anemometer and wind vane respectively at 8 m also showed similar frequency distribution. The profiles of the horizontal wind and temperature observed at 1, 2 and 8 m (using cup anemometer) for low (< 2 ms^{-1}), moderate (5-6 ms^{-1}) and high (> 11 ms^{-1}) wind speeds are presented in the **Figure 4** (a, b and c) respectively. For low and moderate wind speeds, a kink is observed in the wind profile between 2 and 8 m height. For high winds, this kink in the wind profile has gradually disappeared and the profile has become log-linear as observed over a homogeneous terrain. This kink in the wind profiles may possibly be due to change of surface roughness from smooth to rough and the development of internal boundary layer as wind blows from the sea to the land. The IBL height can be determined using equations 1 and 2, assuming, for simplicity, that there is no land-sea temperature difference. The wind profile below the kink represents local surface roughness where as that above it has characteristic of upstream surface (sea). The profile for $U_8 > 11$ ms^{-1} shows a linear increase in wind speed with z, indicating the roughness length of 0.003 m over sea as the kink due to IBL is absent (**Figure 5**). Substituting z_{ol}=0.003 m, b=0.8 and a=0.8 (unstable), the IBL height (δ), from equation 1, is 3.8 m for x=30 m. Thus the kinks in the wind profiles for low and moderate wind speeds indicate that the 1 and 2 m measurement levels on the tower lie within IBL and the 8 m one above IBL. But for high

wind speeds (> 11 ms^{-1}), the IBL is not clearly observed. The reason could be due to prevailing condition of monsoon flow which influences small-scale irregularities like roughness and temperature change at the surface.

In reality there is land-sea temperature contrast at the site. So TIBL develops over the land as monsoon wind blows across the coast. Theory of IBL/TIBL was developed for moderate winds in the absence of synoptic flow. Hence the observed TIBL heights (from kinks in wind and temperature profiles) may differ from those computed from the equations 1 and 3. The computed TIBL height (h) from equation 3, is 4.28 m, assuming $C_D = 3x10^{-3}$; $\theta_1-\theta_s = 2$; x=30 m and γ=9.8°/km. Observed temperature profiles showed inversion above 2 m (Fig. 4). The equations 1 and 3 are applicable for fetches of a few km. In the present case, the fetch is just 30 m. Hence very close to the boundary (a few meters) wind and temperature profiles showed kinks at the same heights, 2 m. Similar to wind profiles, temperature profiles also showed the characteristics of homogeneous terrain (absence of inversions in the profile for unstable conditions) for high wind (> 11 ms^{-1}) conditions (**Figure 4**). However, relative humidity profiles have not shown the tendency to smooth out kinks at high wind speed conditions (not shown). Kinks in the RH profiles existed for low, moderate and high wind conditions. One cannot rely much on RH profiles, as the inherent accuracy of RH sensor is at most 5%. In this case, under high humid conditions (RH 90-100 %) and with measurement levels very close to surface, the small gradients in RH values are insignificant.

6.3 Turbulence Observations

6.3.1 Sonic anemometer

The exchange of the energy between the earth's surface and the atmosphere takes place in the form of turbulence bursts or buoyant plumes in the surface layer. The length scale of turbulence in the surface layer ranges from a few hundred meters (called energy containing range) to a millimeter (called dissipation range). To measure all these eddies of various sizes, sonic anemometer is normally used which measures the rapid fluctuations in wind components (u, v and w) and temperature. One such sonic anemometer (Applied Tech, USA) has been in this field campaign to measure turbulent fluctuations at 10 Hz sampling. The fluctuations (from a mean of 15 minute data record) of vertical wind (dw), temperature (dT) and their instantaneous covariance/kinematic heatflux (w'T') are presented for a typical day for stable and unstable conditions in **Figure 6**. The fluctuations in temperature (dT) were observed to be much more for unstable (July 17, 2002, 1330 IST) condition as compared to that for stable (2200 IST) condition. The fluctuations in w and T are in phase for unstable condition and opposite in phase for stable condition which results in positive heat flux for unstable and negative heat flux for stable conditions.

Sonic anemometer data on July 24, 2002 were analyzed to calculate 30-min mean values of sensible heat flux, friction velocity, three wind components and temperature. Diurnal variation of these parameters is shown in **Figure 7**. Vertical wind shows strong down drafts in the day time in spite of positive heat flux. This unusual feature, observed on this particular day, needs to be clarified with further analysis of the entire data. The sharp

drop in air temperature by 2° C at around 0400 hr IST is associated with a change in the direction of u-component from southerly (u is +ve) to northerly (u is –ve) and an increase in wind speed from 3.0 to 5.5 ms^{-1}.

The data during the period 13-28 July were used to check the characteristic features of turbulence. **Figure 8(i)** shows the standard deviation of wind components σ_u, σ_v and σ_w normalized with the friction velocity u_*. It can be seen that $\sigma_u / u_* = 2.5$, $\sigma_v / u_* = 1.5$ and $\sigma_w / u_* = 1.25$, for near neutral conditions. The large scatter in horizontal velocity components are probably due to the influence of large scale circulation on boundary layer during monsoon. **Figure 8(ii)** depicts correlation of vertical wind with temperature and u-component as a function of static stability z/L where z is the height of measurement and L, Monin-Obukhov length. The correlation coefficient Cor_{wT} was found to be ~ 0.4 for unstable (- z/L) condition (Kaimal and Fennigan, 1994). Large scatter was observed for stable conditions. Sensible heat flux showed diurnal variation from –50 to 150 wm^{-2}. Kinematic momentum flux was observed to have large scatter (0 to –0.4 m^2s^{-2}) with an average of ~ -0.2 m^2s^{-2}.

Spectra of turbulence provide useful information on the scales of motion that contribute to the production and dissipation of energy. The spectra of wind and temperature are shown in **Figure 9** (a, b) on July 26 for unstable (z/L= -0.046) and stable (z/L= 0.011) atmospheric conditions. Characteristic inertial subrange slope of –2/3 was observed in the spectra of three wind components and temperature. A little deviation from –2/3 slope was observed in temperature spectrum at f > 1 Hz for stable condition. According to *Taylor's 'Frozen turbulence'* theory, if the lifetime of an eddy is more than the time it takes to move past the point of measurement, then the spatial and temporal variations in turbulence statistics are interchangeable. Hence $u = f \lambda$, where u is the wind component in the mean wind direction, f is the frequency and λ is the wavelength or eddy size. Well –defined peak was not observed in u-spectrum for unstable condition (**Figure 9**). By drawing a smooth line to fit the observations, the frequency f corresponding to the peak in $fS_u(f)$ is ~ 0.08 Hz. The approximate eddy size (corresponding to a sampling time of 7 minutes or 4096 points) that contributes maximum for turbulence kinetic energy or the integral length scale (l) will be u/f, that is ~ 59 m. Sensible heat flux, friction velocity and air temperature corresponding to unstable condition are also shown in the **Figure 9a**. Similarly for stable condition (**Figure 9b**), the integral length scale, l, was observed to be ~ 35 m (u=5.3 ms^{-1}, $f_{peak} = 0.15$).

Time series of half-hourly mean sensible heat flux, estimated by eddy correlation technique using sonic anemometer data, are presented in **Figure 10** along with daily rainfall for the period July13-28. One can observe the fluctuations in sensible heat flux in terms of rainfall. The sudden drop in sensible heat flux on July 15-16 and rise on July 17 is associated with a daily rainfall of 25-40 mm on July 15-16 and 2 mm rainfall on July 17. The period July 18-23 experienced continuous rainfall of ~ 10 mm daily which has resulted in relatively low sensible heat flux during this period. These observations will be useful to study the thermodynamic instability in the ABL along with upper air observations.

6.3.2 H_2O/CO_2 Gas Analyzer

The water vapour and carbon dioxide densities measured by H_2O/CO_2 open path gas analyzer or InfraRed (IR) Hygrometer at 10 Hz were averaged to get 30-minute mean densities. Sonic anemometer measurements of vertical wind were synchronized with water vapour density measurements and used to compute latent heat flux by eddy-correlation technique. Time variation of H_2O and CO_2 densities are shown in Figure 11 for a typical day, September 20. Water vapour (H_2O) and CO_2 densities were observed to be in the range of 18 – 23 gm m^{-3} and 550 – 750 mg m^{-3} respectively. Since 1 ppm = 1.796 gm m^{-3} for CO_2, its concentration was observed to be about 350 ppm at the site. An inverse relationship between H_2O and CO_2 densities can be seen on some instances, for example, from 1200 hr IST water vapor density began to increase while CO_2 density started falling (**Figure 11**). But during 0900-1100 hr IST, they are in same phase, both increasing with time. Since water vapor density (ρ_{water}) can vary with air temperature and advection of moisture, wind components and air temperature derived from sonic anemometer (Figure 12) are used to explain the variations in water vapor concentration. ρ_{water} was ~ 22.5 gm m^{-3} during 0000-0700 hr IST and it began dropping 0700 hr IST and became ~ 21.5 gm m^{-3} at 0900 hr IST. This reduction during 0700-0900 hr IST is associated with rising air temperature after Sunrise (**Figure 12**). The sudden rise in ρ_{water} at 0900 hr IST can be attributed to change in wind (u-component) direction from northerly (u -ve) to southerly (u +ve) at 0900 hr IST (**Figure 12**) that brings moisture from the sea. With southerly winds blowing from the sea, air temperature also dropped suddenly from 26 C at 0900 hr to 25 C at 1000 hr IST. These southerly winds lasted until 1130 hr IST and so the temperature remained low. From 1130 hr IST, wind slowly changed from southerly towards northerly which is associated with gradual rise in air temperature (**Figure 12**). The rise of ρ_{water} from 1200 hr IST onwards is due to increase in evaporation associated with heating of the ground by solar radiation (**Figure 11**). The rise in CO_2 density during 0900-1100 hr IST could possibly be due to advection of smoke from the sailing fishermen boats/ships off the coast (**Figure 11**). Diurnal variation of CO_2 flux and sensible, latent heat fluxes on September 20 are shown in **Figure 13** (a, b). Negative flux of CO_2 was observed as sea is a known sink of atmospheric CO_2. CO_2 flux showed maximum during noon hours with a magnitude of – 1.4 mg $m^{-2}s^{-1}$ on September 20. This is substantially less as compared to that over a forest which is ~ 1 gm $m^{-2}s^{-1}$. Latent heat flux maximum was observed to be ~ 350 wm^{-2} around 1000 hr IST and is double that of sensible heat. It is less than sensible heat flux by ~ 100 wm^{-2} during noon hours on September 20 (**Figure 13**). Latent heat flux showed fluctuations unlike sensible heat flux during 1200-1600 hr IST. More data have to be analyzed to know the order of magnitude of representative latent heat flux at this coastal site. **Figure 14** presents the time series of half-hourly mean densities of water vapour, carbon dioxide and atmospheric pressure during the period August 1-31, 2002. Diurnal as well as low frequency oscillation of pressure can be seen in the plot. Much larger fluctuations (spikes) in carbon dioxide and water vapour densities are due to precipitation/drizzle. The order of carbon dioxide density is ~ 300 ppm (600 mg m^{-3}) and that of water vapour is 23 gm m^{-3} (**Figure 14**) during August 2002.

The spectrum of water vapour for stable and unstable conditions are presented for July 24 in **Figure 15** that depicts the –2/3 slope in the inertial subrange. The magnitude of $fS_q(f)$ for unstable condition is much higher than that for stable condition. There are three prominent frequency peaks i.e., 3 and 1 minute, the latter has more spectral density. Also there exists a peak of 4-5 seconds which correspondent to intermittent turbulence in buoyancy. The vertical velocity spectrum also shows a peak at this frequency in Figure 9a for unstable condition. It can be seen that this peak is absent in stable condition (Figure 9b). The spectrum for stable condition show many peaks, however we shall identify 3, 1 minute peak and 30 second peak having nearly same spectral density. However, more spectra have to be analyzed.

6.4 Slow/conventional sensors

Conventional sensors/instruments like cup anemometer, temperature and humidity instruments have been used to measure profiles of meteorological parameters in the atmospheric surface layer and a tipping bucket rain gauge for recording rainfall. These data are available at 1 minute interval. A precipitation event on July 20 has been analyzed to study the response of these instruments. **Figure 16** presents the time variation of half-hourly mean wind, humidity, temperature and radiation on July 20. Rainfall of 10 mm had occurred a few minutes past 1200 hr IST on this day. It can be inferred from this figure that gusty wind of ~ 8 ms^{-1} prevailed at the time of precipitation which has subsequently reduced to its normal strength. Solar radiation (shortwave incoming, sw-in) was ~ 400-600 wm^{-2} during 0800-1030 hr IST showing that the sky is partly cloudy on this day. Further reduction in solar radiation continued till the precipitation. Solar radiation reached to a maximum of 1000 wm^{-2} at 1330 hrs just after precipitation. Air temperature and relative humidity followed according to the variation of short wave radiation. Interestingly before and after the disturbed weather due to precipitation, the air temperature showed maxima. The rapid changes in air temperature and relative humidity before and after the rainfall show the sensitivity of surface layer to precipitation.

7. Conclusions

The data generated by IITM team during ARMEX at the NCAOR site at Vasco-Da-Gama have been used to study the profiles and fluxes in the atmospheric surface layer. The following conclusions are drawn from the study.

- There exists an internal boundary layer (IBL) extending up to about 4 m from the surface. Hence the fluxes measured directly above this height at 5 m level on the tower shall represent coastal surface fluxes.

- Turbulence statistics of wind, temperature, heat and momentum follow the universal similarity relations of the atmospheric surface layer.

- Prominent energy peaks (period 4-5 sec.) in the spectrum (sampling time: 7 min.) of temperature, water vapor and vertical velocity in unstable conditions show intermittency in turbulence due to buoyancy. The inertial subrange in the spectra of wind, temperature and water vapor depict -2/3 law of Kolmogorov.

- An analysis of a precipitation (10 mm) event during noon time showed rapid changes in short wave solar radiation, surface wind, air temperature and relative humidity before and after the precipitation indicating the sensitivity of the surface layer to precipitation.

- An inverse correlation seems to exist between daily rainfall and sensible heat flux.

Acknowledgements

The authors would like to thank the Department of Science & Technology, Government of India for funding this project. It is a pleasure to thank Shri D.R.Sikka, Chairman, ICRP and Prof. Mrs.Sulochana Gadgil, IISC,Bangalore, for their interest in evolving the program ARMEX. We gratefully acknowledge with thanks the keen interest shown, whole hearted support and kind encouragement given by Dr.G.B.Pant, Director, Indian Institute of Tropical Meteorology, Pune to this field programme. We extend our hearty thanks to Dr.P.C.Pandey, Director, National Centre for Antarctic & Ocean Research (NCAOR),Vasco-Da-Gama, Goa, for his interest in the campaign and the infrastructure facilities at NCAOR. Our sincere thanks to Dr Bhaskara Rao, and Dr Sudhakar, Group Directors, NCAOR for their kind help and coordination during the field campaign. We acknowledge the staff members of NCAOR for their kind cooperation. We extend our thanks to Dr Sanjeeva Rao, Scientist, DST for the help and administrative support to the programme. We are thankful to IMD, Pune for extending their calibration facility. We thank Shri.S.Sinha, Head, BLLSPS, Division, IITM for the interest and cooperation. We also wish to thank the referee Dr T.Venugopal, IITM for his useful suggestions and comments on this report.

8. References

ARMEX, Science Plan - Indian Climate Research Programme, August 2001: Department of Science & Technology, Government of India, New Delhi.

Beljaars, A.C.M., 1987: On the memory of wind standard deviation for upstream roughness, Bound.-Layer Meteor., 38, 95-102.

Garratt J.R., 1990 : The Internal Boundary Layer – A Review, Boundary-Layer Meteorology, 50, 171-203.

Hsu, S.A., 1986: A note on estimating the height of the convective internal boundary layer height near shore. Boundary-Layer Meteorol., 35, 311-316.

Kaimal,J.C., and J.J.Finnigan, 1994:Atmospheric Boundary Layer Flows;Their Structure and Measurement, Oxford University Press, New York.

Panofsky, H.A., D.Larko, R.Lipschutz, G.Stone, E.F.Bradley, A.J.Bowen, J.Hojstrup, 1982 : Spectra of velocity components over complex terrain. Quart.J.Roy.Meteor.Soc., 108, 215-230.

Rao, K.S., J.C.Wyngaard and O.R.Cote, 1974 : The structure of the two-dimensional internal boundary layer over a sudden change of roughness. J.Atmos.Sci., 31, 738-746.

Raynor G.S., Michael P., Brown R.M., and Sethuraman S., 1975: Studies of atmospheric diffusion from a near shore oceanic site. J.Appl.Meteorol., 14, 1080-1094.

Raynor G.S., Sethuraman S, and Brown R.M., 1979: Formation and characteristics of coastal internal boundary layers during onshore flows. Boundary-Layer Meteorol., 16, 487-514.

Smedman-Hogstrom, A.S., and Hogstrom, 1978 : A practical method for determining wind frequency distributions for the lowest 200 m from routine meteorological data. J.Appl.Meteor., 17, 942-954.

Stull R.B., 1988: Introduction to Boundary Layer Meteorology, Kluwer Academic Publisheres, The Netherlands.

Venkatram, A., 1977: A model of Internal Boundary-Layer Development, Boundary-Layer Meteorol., 11, 419-437.

Appendix A

Sensors/instruments used in the field experiment at Vasco, Goa.

Parameter	Sensor/Instrument	Range	Accuracy
Wind speed	3 cup anemometer	0-65 m/s	+/- 2% of FSR
Wind direction	Potentiometric wind vane	0-357 deg.	+/- 2 deg.
Air temperature	Platinum resistance thermometer	-40 – 60 C	+/- 0.1 C
Relative humidity	Solid state capacitance type	0-99%	2% of FSR
Solar Radiation	Radiometers (Eppley)	0.3 to 3 μm & 3 to 60 μm	
Rainfall	Tipping bucket Rainguage	unlimited	1 mm

Sonic anemometer

The sonic anemometer manufactured by Applied Tech., USA, is a solid-state ultrasonic instrument capable of measuring wind velocities in three orthogonal axes (U, V and W) and sonic temperature. The sonic anemometer is comprised of a probe array whose sonic transducers are separated by 15 cm. Sonic pulses are generated at the transducers and are received by opposing transducers. Mathematics derived for these sonic pulses provide a wind velocity measurement in each of the corresponding axes and provides a sonic temperature which is generated from the data in the "W" axis. The velocity measurements are corrected for flow distortion and the sonic temperature is corrected for velocity contamination.

Measurement range :	Wind velocity : 15 m/s	Temperature : -20 to +50 C
Accuracy :	Wind speed : +/- 0.05 m/s Sonic temperature : +/- 0.05 C	Direction : +/- 0.1 deg.
Resolution :	Wind speed : 0.01 m/s Temperature : 0.01 C	Wind direction : 0.1 C

u component denotes the *South-North component of wind* which is *positive* when the wind is from *South to North* and vice-versa.
v component denotes the *East-West component of wind* which is *positive* when the wind is from *East to West* and vice-versa.
Hence for *South-Westerly* wind, *u component* should be *+ve* and *v component –ve.*
w component denotes *Vertical wind* which is *positive* when it is upward (*updraft*) and vice-versa.

H_2O/CO_2 Open Path Gas Analyzer / Infrared Hygrometer (LI-7500)

The LI-7500 is a high performance, non-dispersive, open path infrared H_2O/CO_2 Analyzer designed for use in eddy covariance flux measurement systems. It makes simultaneous measurements of CO_2 and H_2O at high speeds in the free atmosphere. Internal 150 Hz measurements are digitally filtered to provide a true 5, 10 or 20 Hz bandwidth. It can be configured using a windows software. It outputs analog as well as digital data. The output consists of densities CO_2 (mg/m^3 and $mmol/m^3$) and H_2O(gm/m^3 and $mmol/m^3$).

Gill propeller anemometer

The Gill propeller anemometer, manufactured by Young Inc., UK, is mutually orthogonal three axis propeller anemometer that measures wind components in three perpendicular directions (u, v and w). The output is in volts which can be converted to wind speed in ms^{-1} using the calibration curves. The blades of the anemometer are very light and have less threshold compared to that for cup anemometers. The analog output can be sampled at 10 Hz and be used along with any scalar to estimate the vertical flux of the scalar using eddy correlation technique provided both the signals are synchronized in time to an accuracy of less than 0.1 sec.

In this field campaign, PCL208 A/D card has been used to sample the analog signals from the Gill propeller anemometer and H_2O/CO_2 Analyzer simultaneously. The software provided with the card has been used to configure the data acquisition setup.

It is oriented parallel to the sonic anemometer at the same height.
u component denotes the *North-South component of wind* which is *positive* when the wind is from *North to South* and vice-versa
v component denotes the *East-West component of wind* which is *positive* when the wind is from *East to West* and vice-versa.
Hence for *South-Westerly* wind, *u component* should be *-ve* and *v component –ve.*
w component denotes *Vertical wind* which is *positive* when it is upward (*updraft*) and vice-versa.

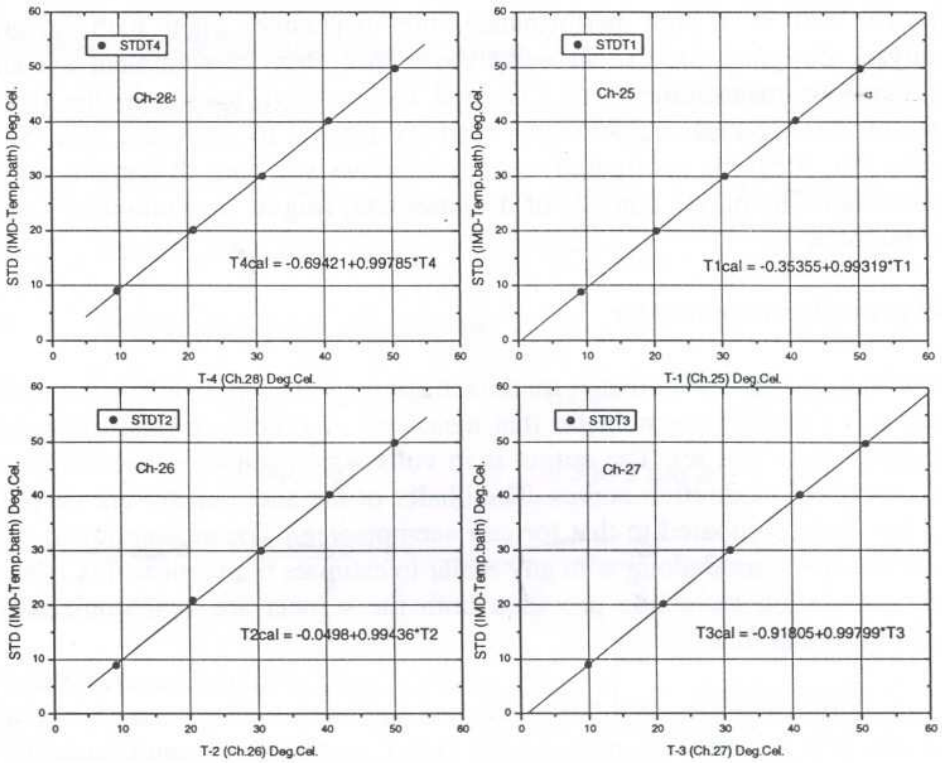

Tempearture sensor calibration in IMD's Temp-bath.

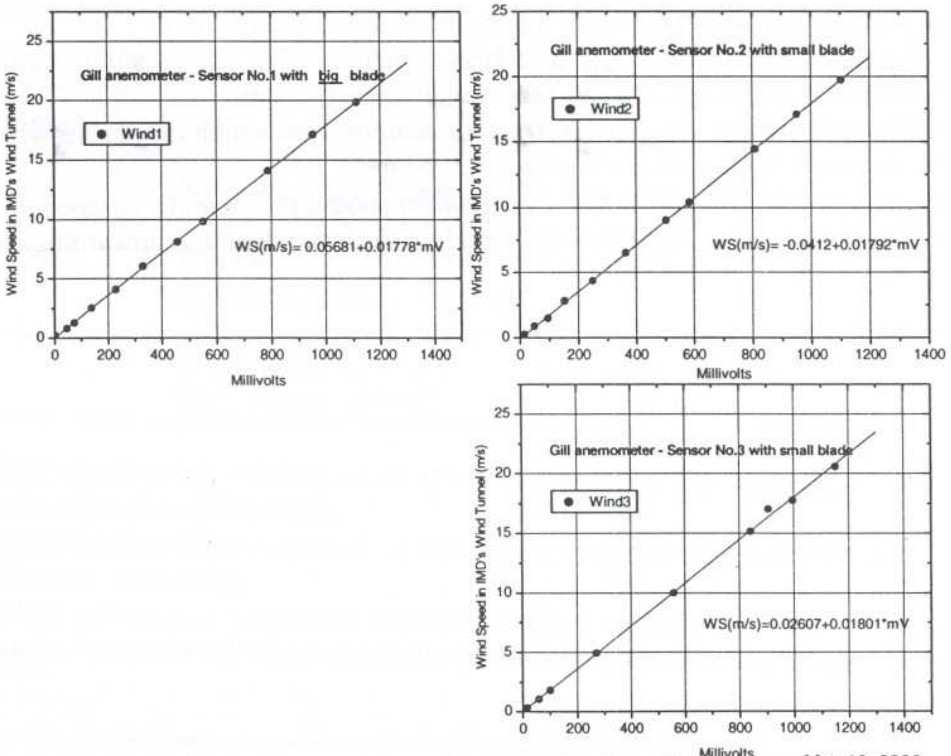

Calibration of Gill propeller anemometer in IMD's Wind Tunnel May 10, 2002

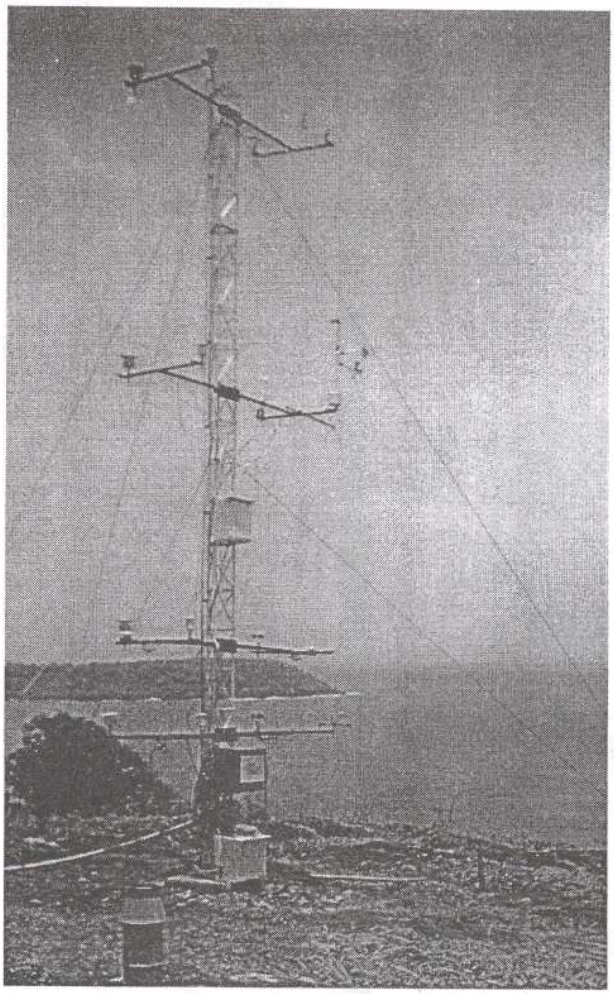

Fig. 1 Meteorological Tower on the west coast of India at Vasco-Da-Gama, Goa, India.

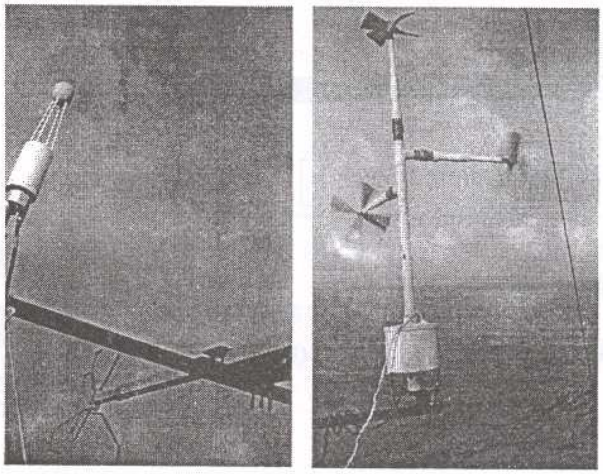

Fig. 1b : A close view of CO_2/H_2O Analyzer, Sonic anemometer and Gill Propeller anemometer (L to R)

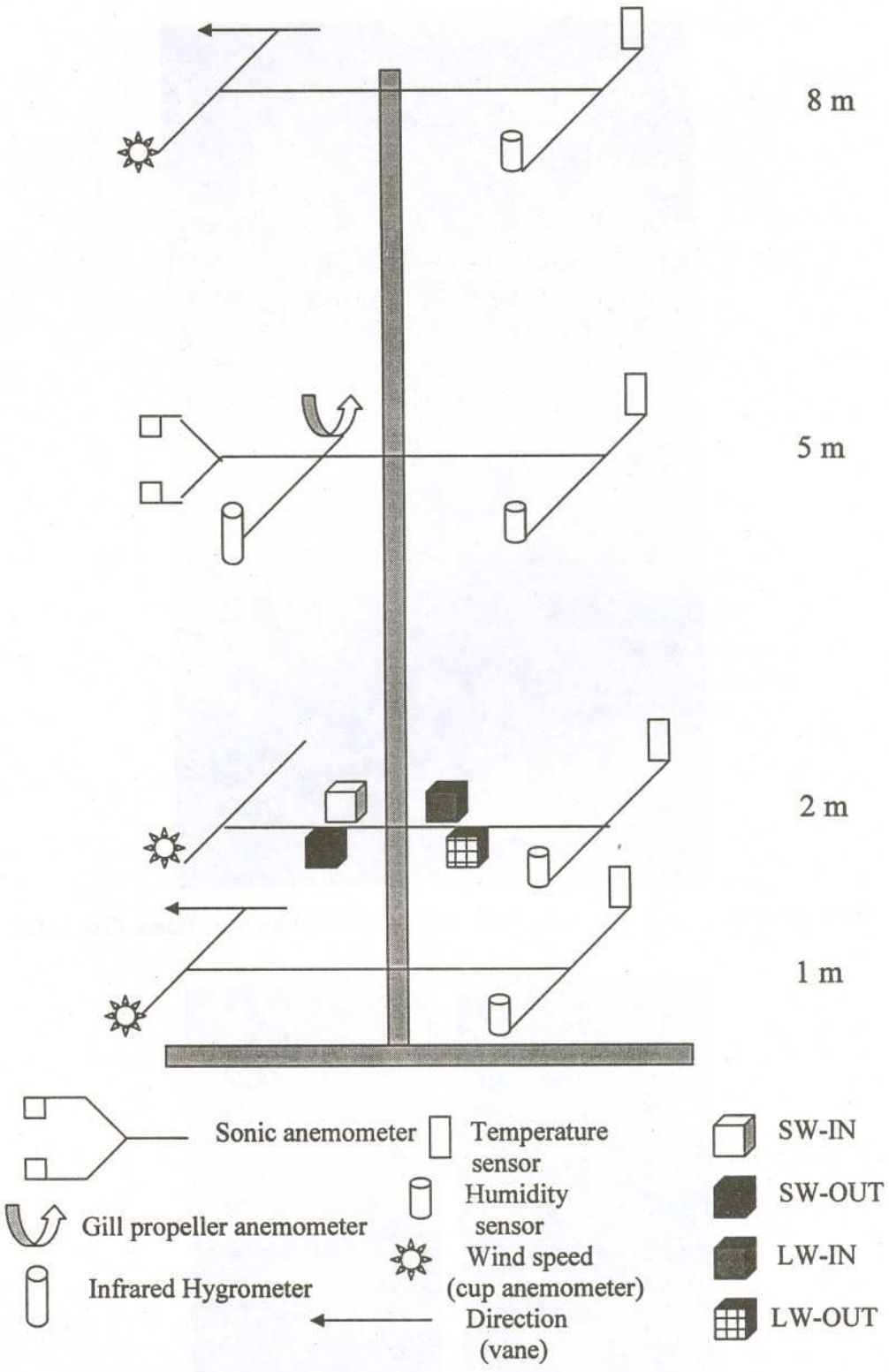

Fig. 2 Schematic diagram of the experimental setup at Vasco, Goa

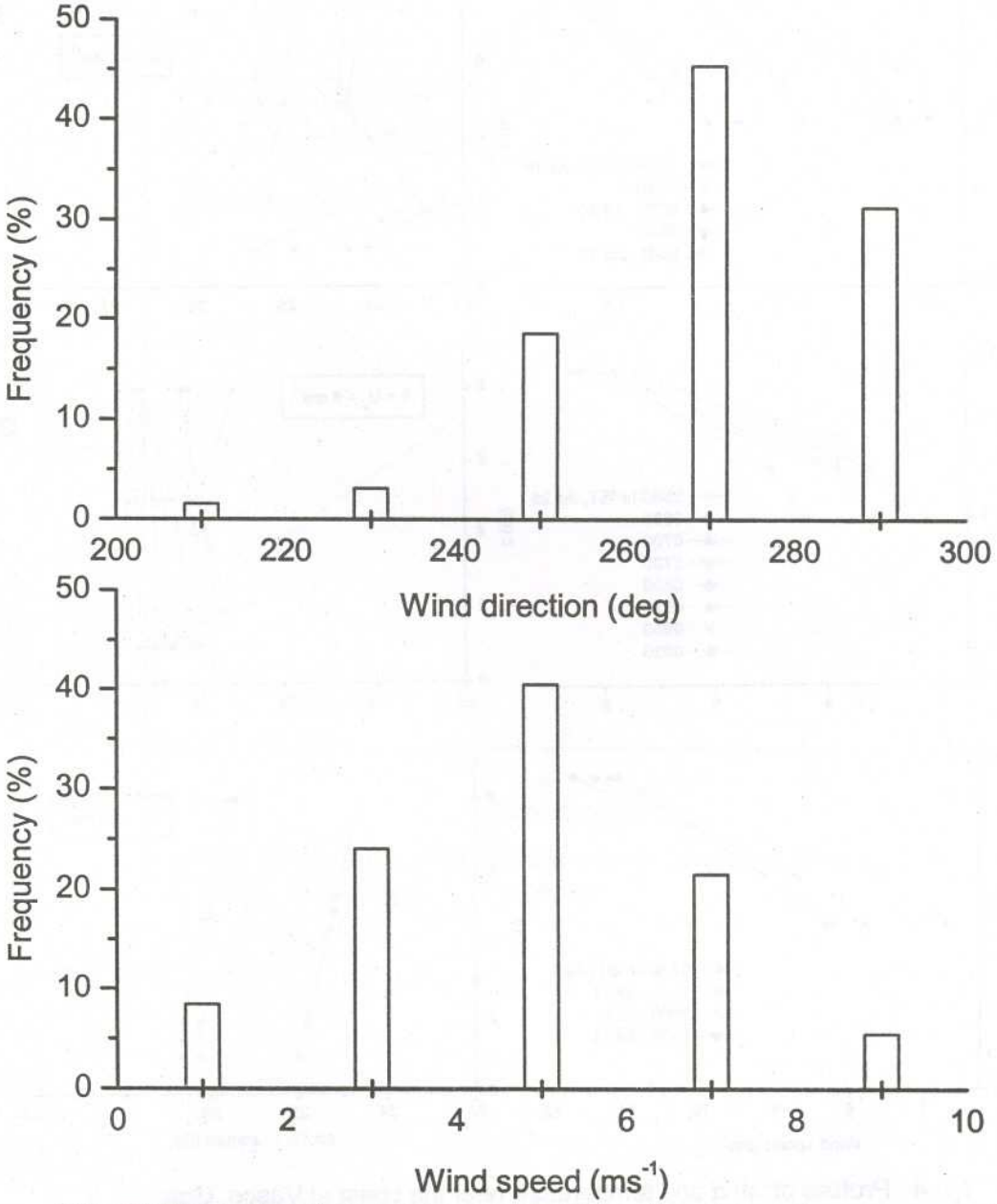

Fig.3 Wind direction and speed at 5 m level (sonic anemometer) during July 13-28, 2002

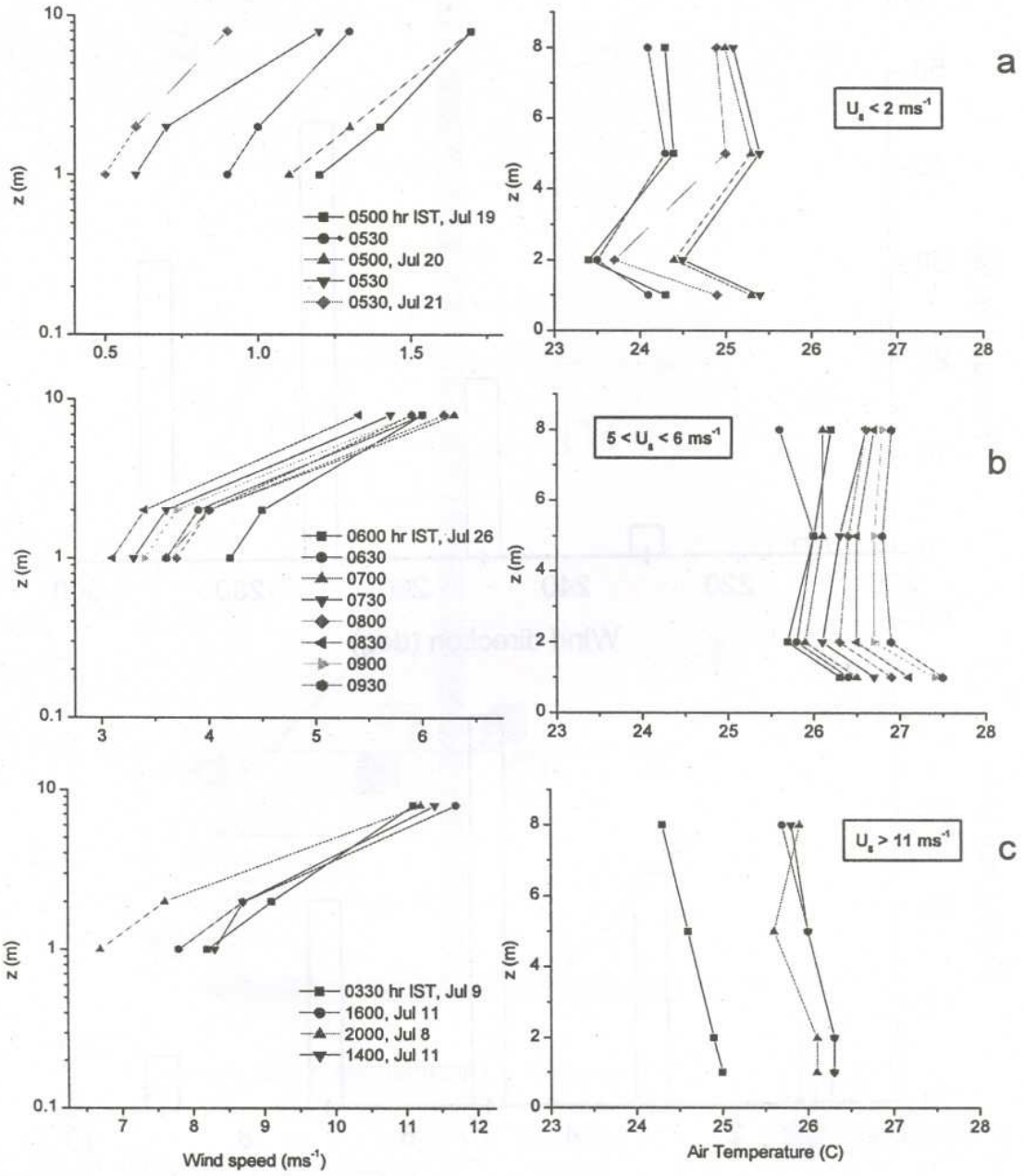

Fig.4 : Profiles of wind and temperature near the coast at Vasco, Goa

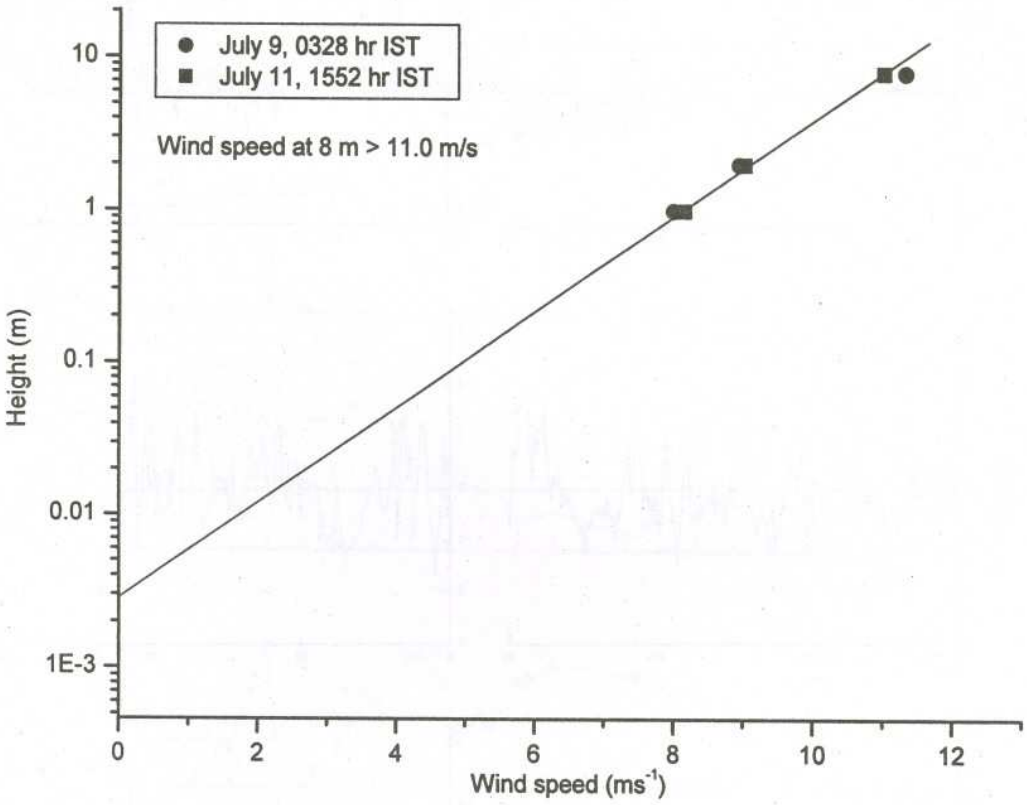

Fig. 5 Log-linear wind profile for high wind (> 8 ms^{-1}) conditions. Roughness length, z_{o1} = 0.003 m

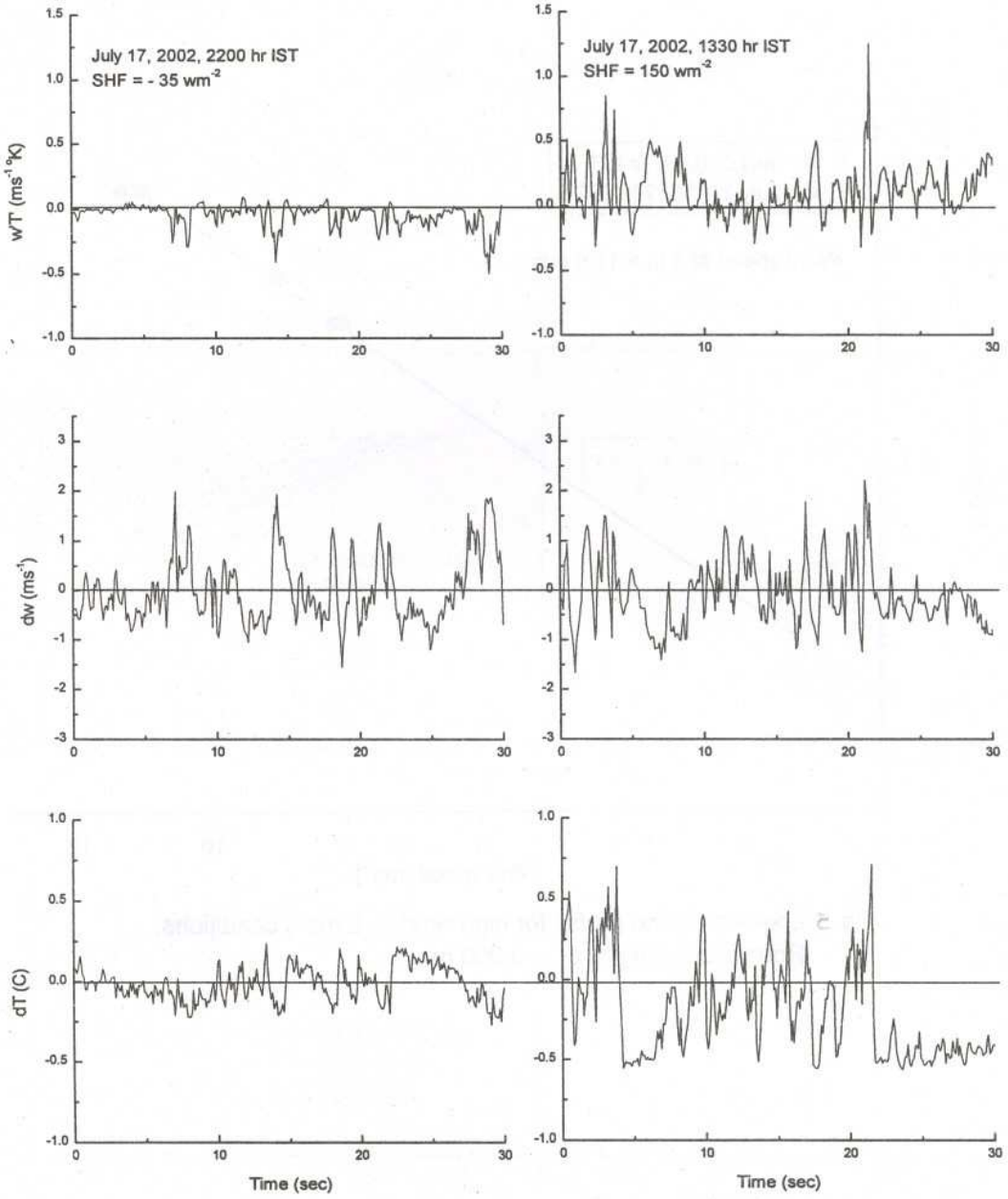

Fig.6 Time series of fluctuations of air temperature (dT), vertical velocity (dw) and kinematic heat flux (w'T') as measured by sonic anemometer for stable and unstable conditions

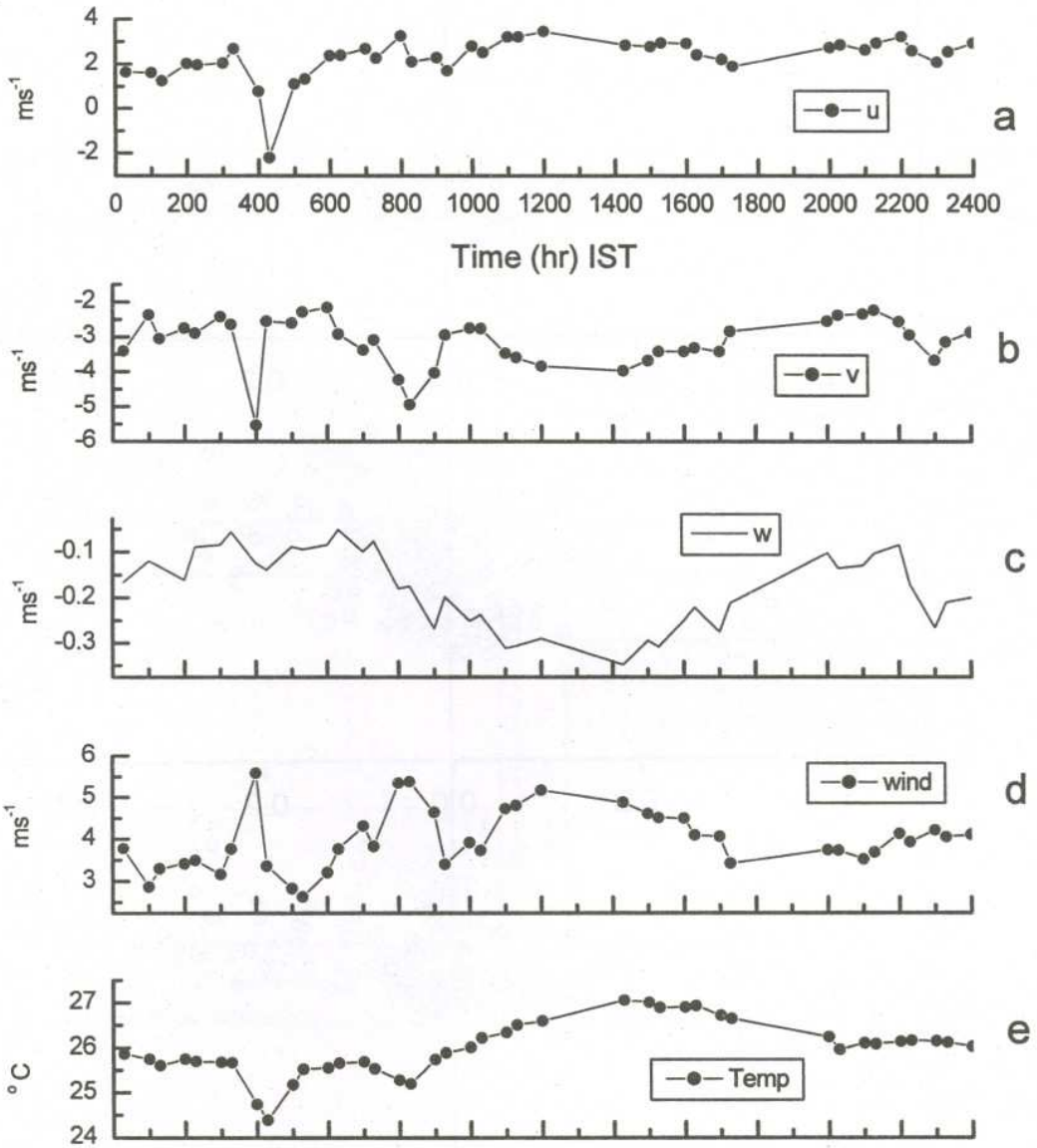

Fig.7 Diurnal variation of u (a), v (b), w (c), wind (d) and temperature (e) on July 24, 2002 as observed by sonic anemometer at 5m.

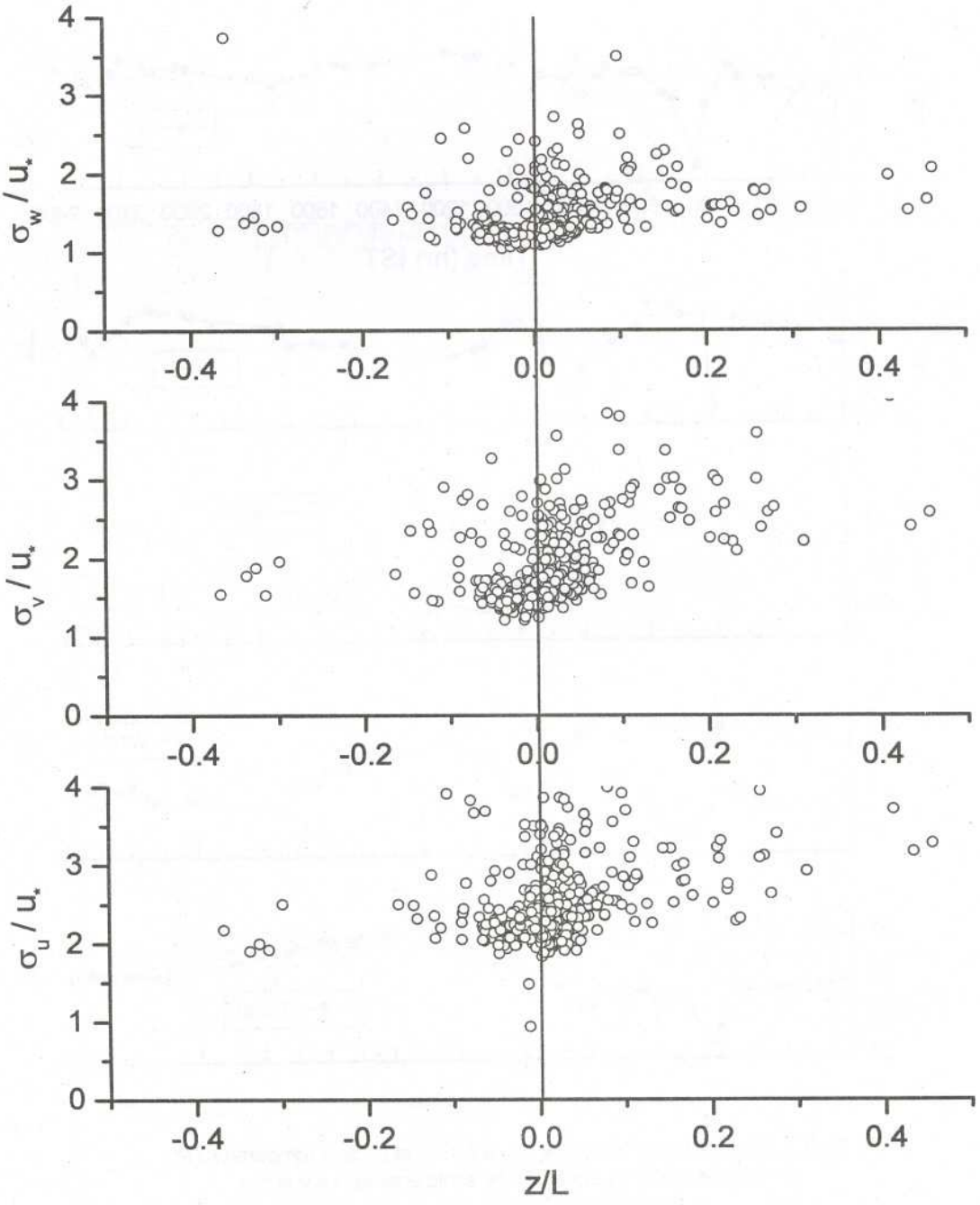

Fig.8(i) Standard deviations of wind components normalized with friction velocity as a function of stability parameter during July 13-28, 2002

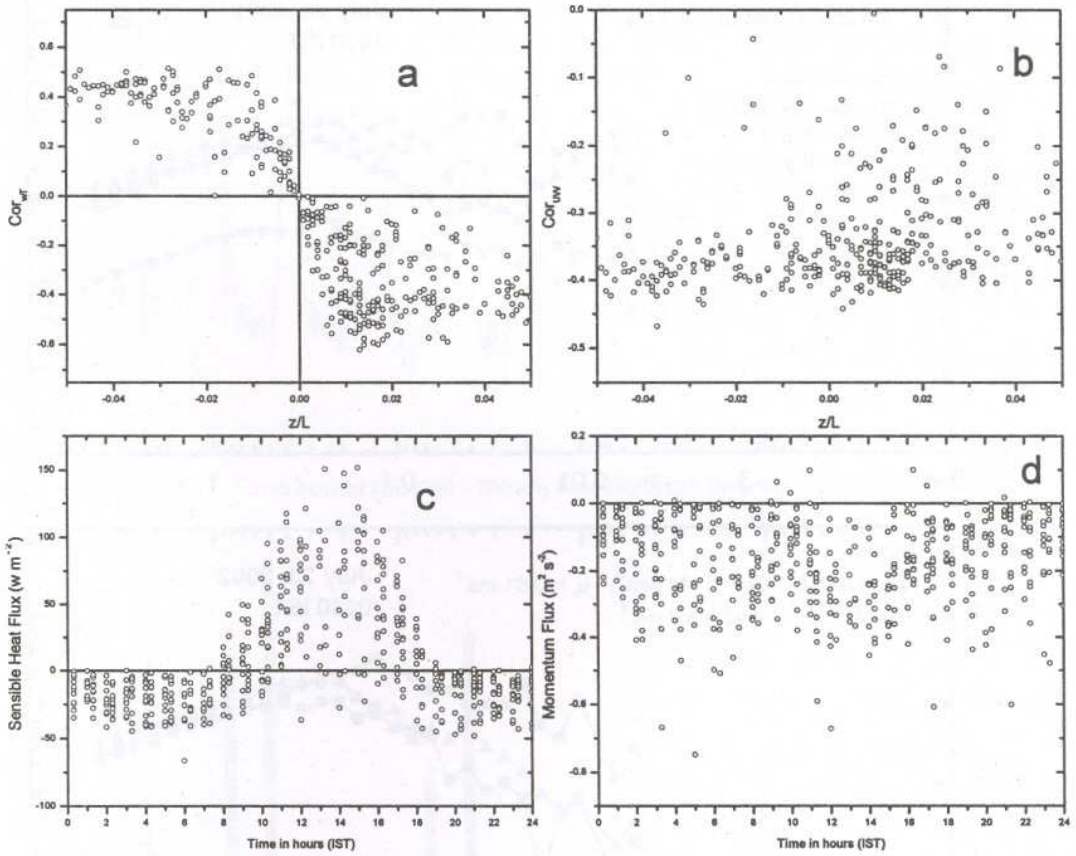

Fig.8(ii) Correlation coefficients (a) Cor_{wT}, (b) Cor_{uw}, (c) sensible heat flux and (d) Momentum flux during 13-28 July, 2002

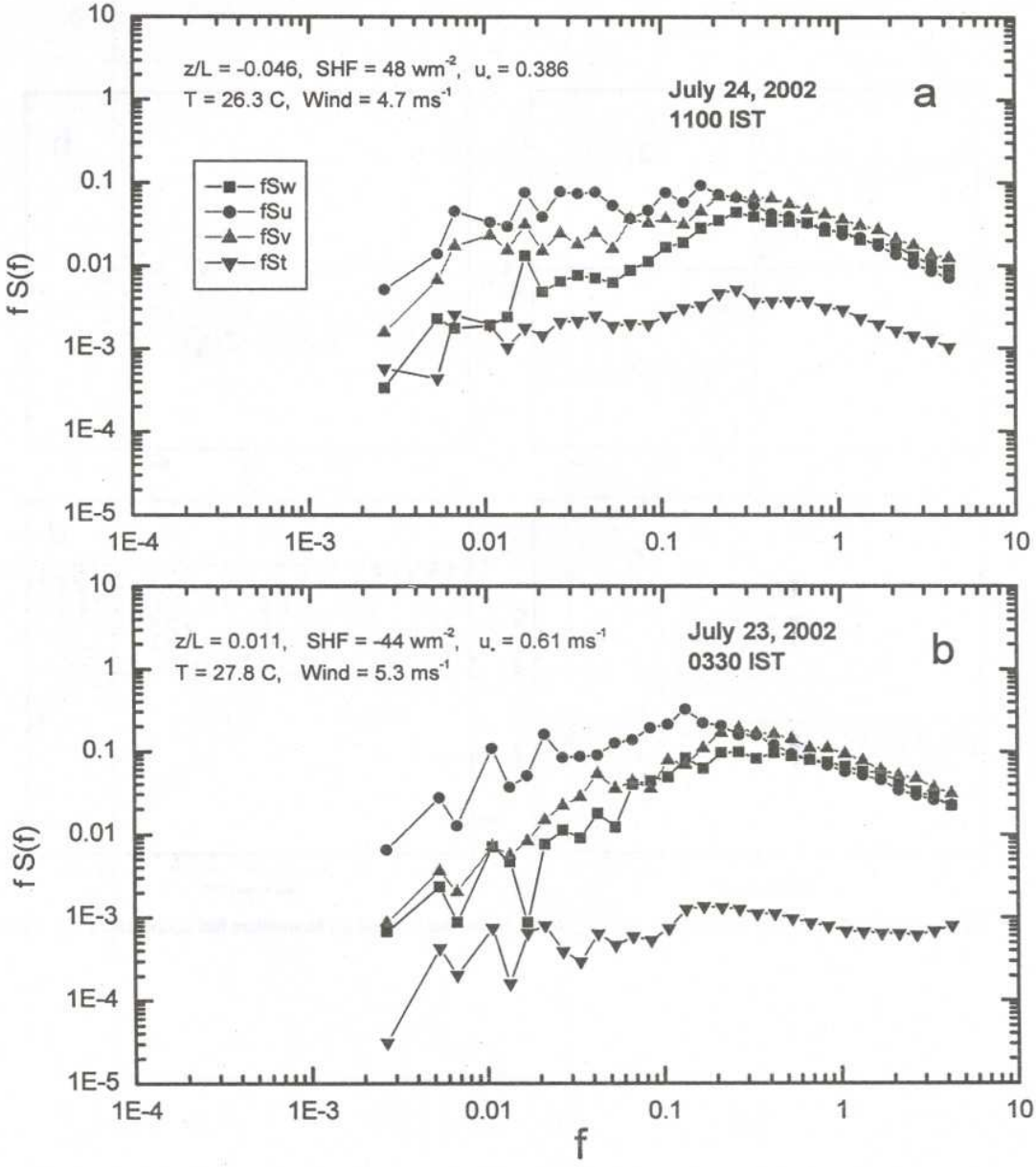

Fig.9 Spectra of u, v, w, T for (a) unstable and (b) stable atmospheric conditions

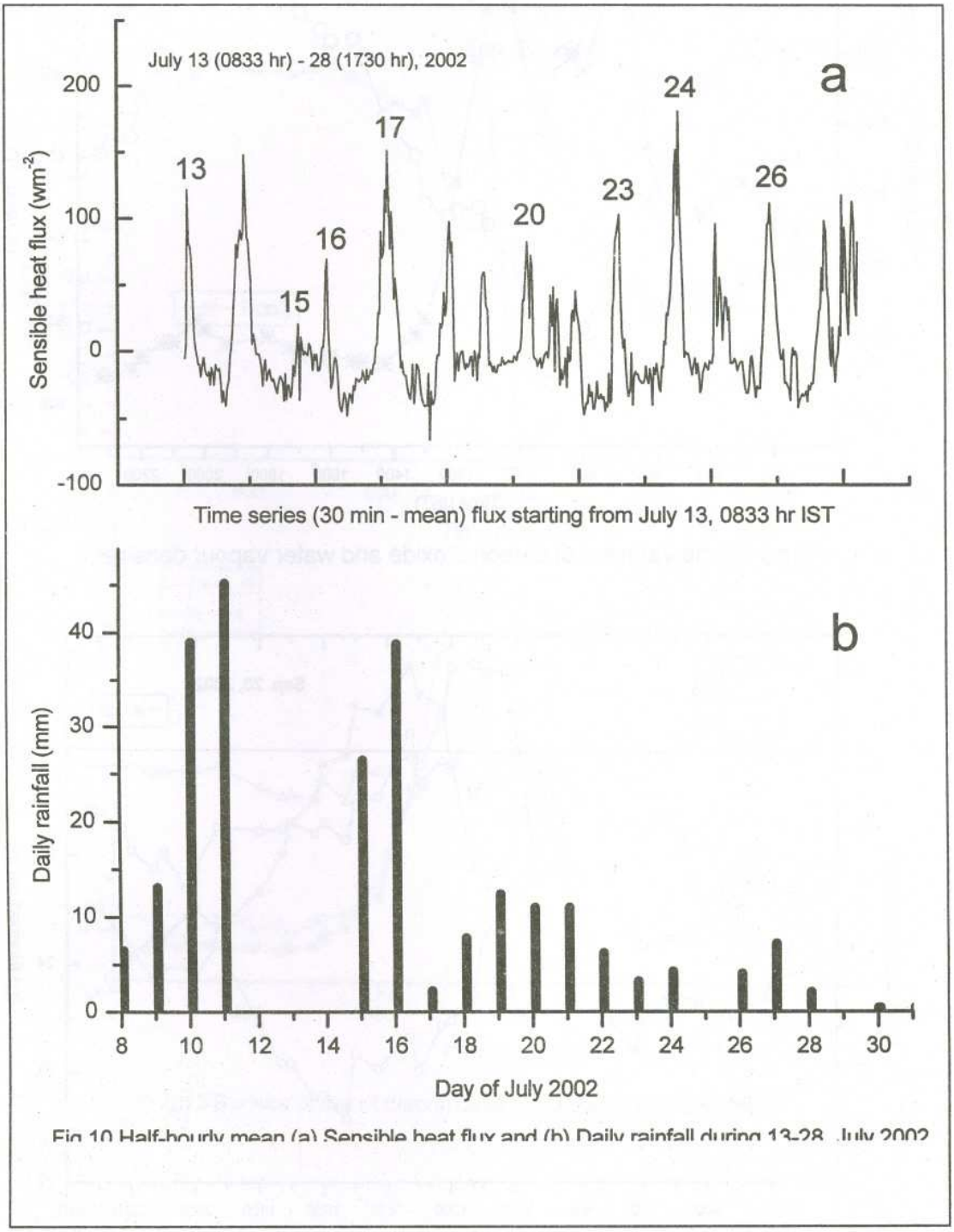

Fig 10 Half-hourly mean (a) Sensible heat flux and (b) Daily rainfall during 13-28 July 2002

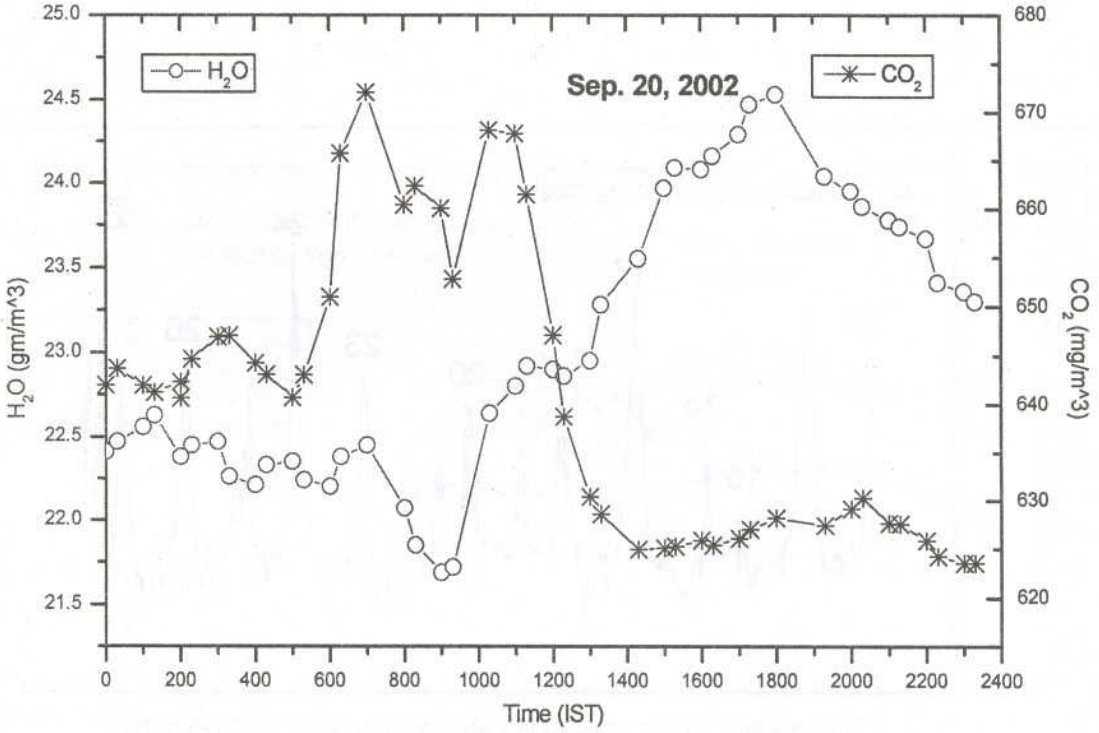

Fig.11 Time variation of carbon dioxide and water vapour densities.

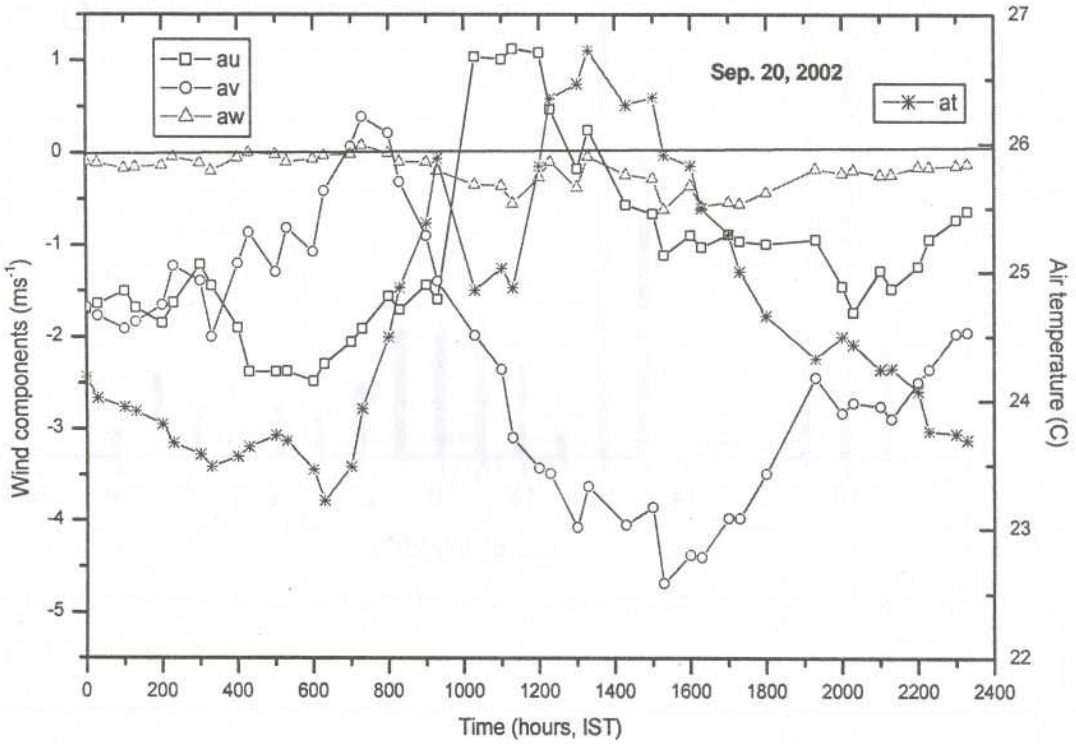

Fig.12 Time variation of wind and temperature measured by sonic anemometer

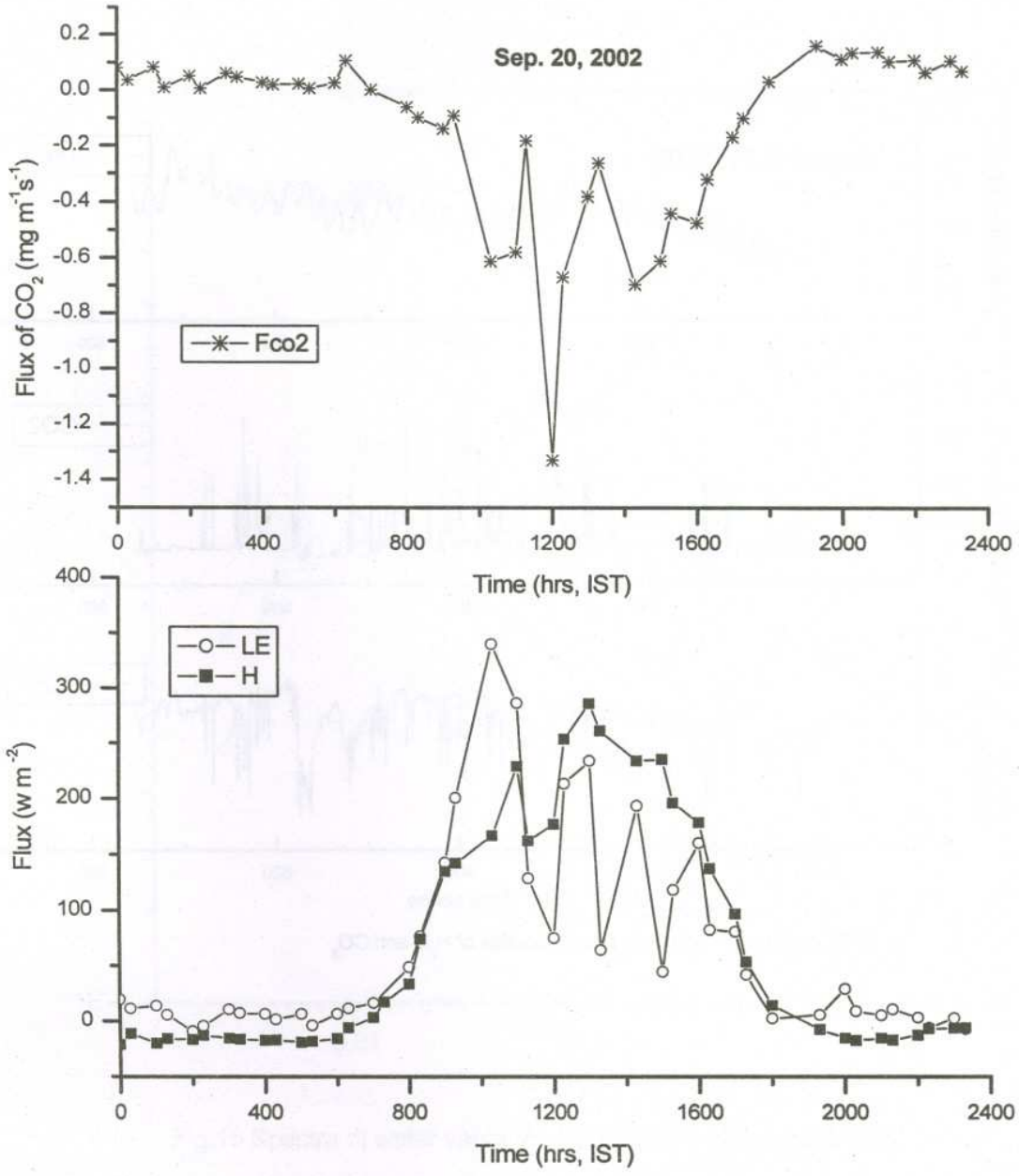

Fig.13 Surface fluxes of carbon dioxide, sensible and latent heat.

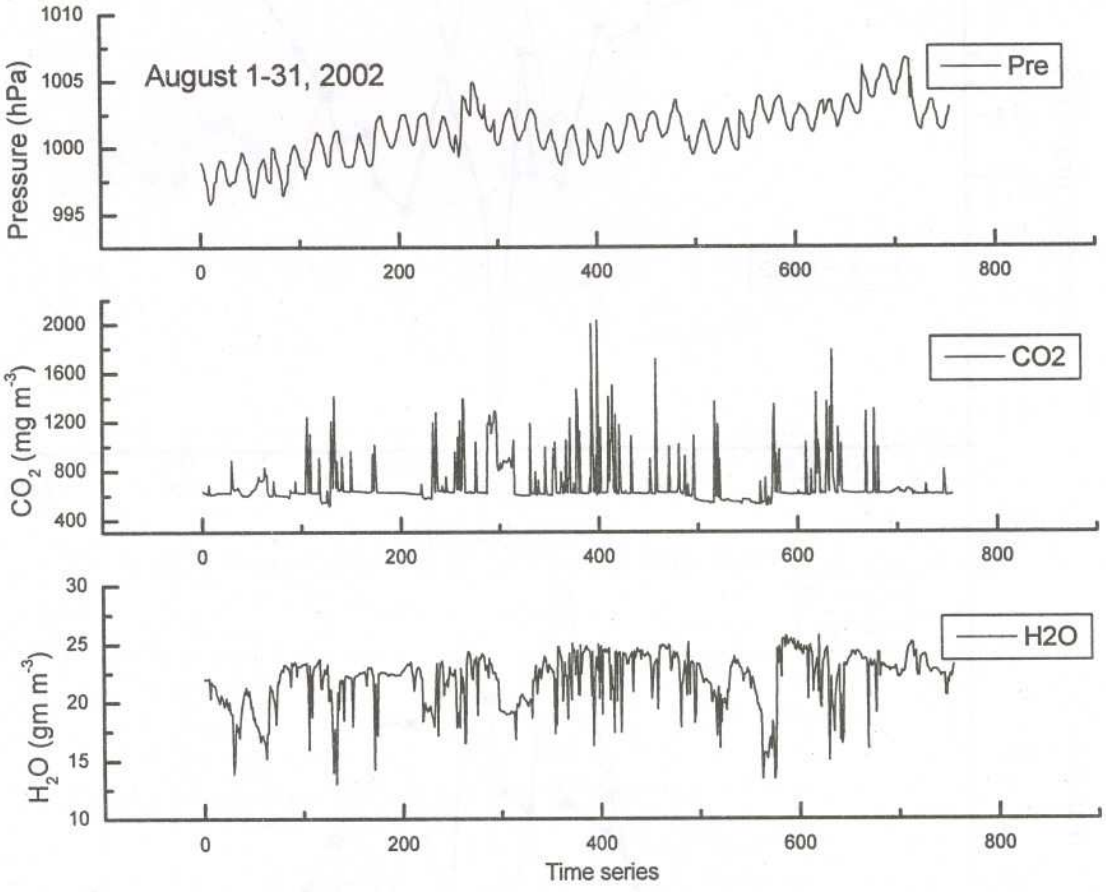

Fig.14 Time series of half-hourly mean densities of H_2O and CO_2

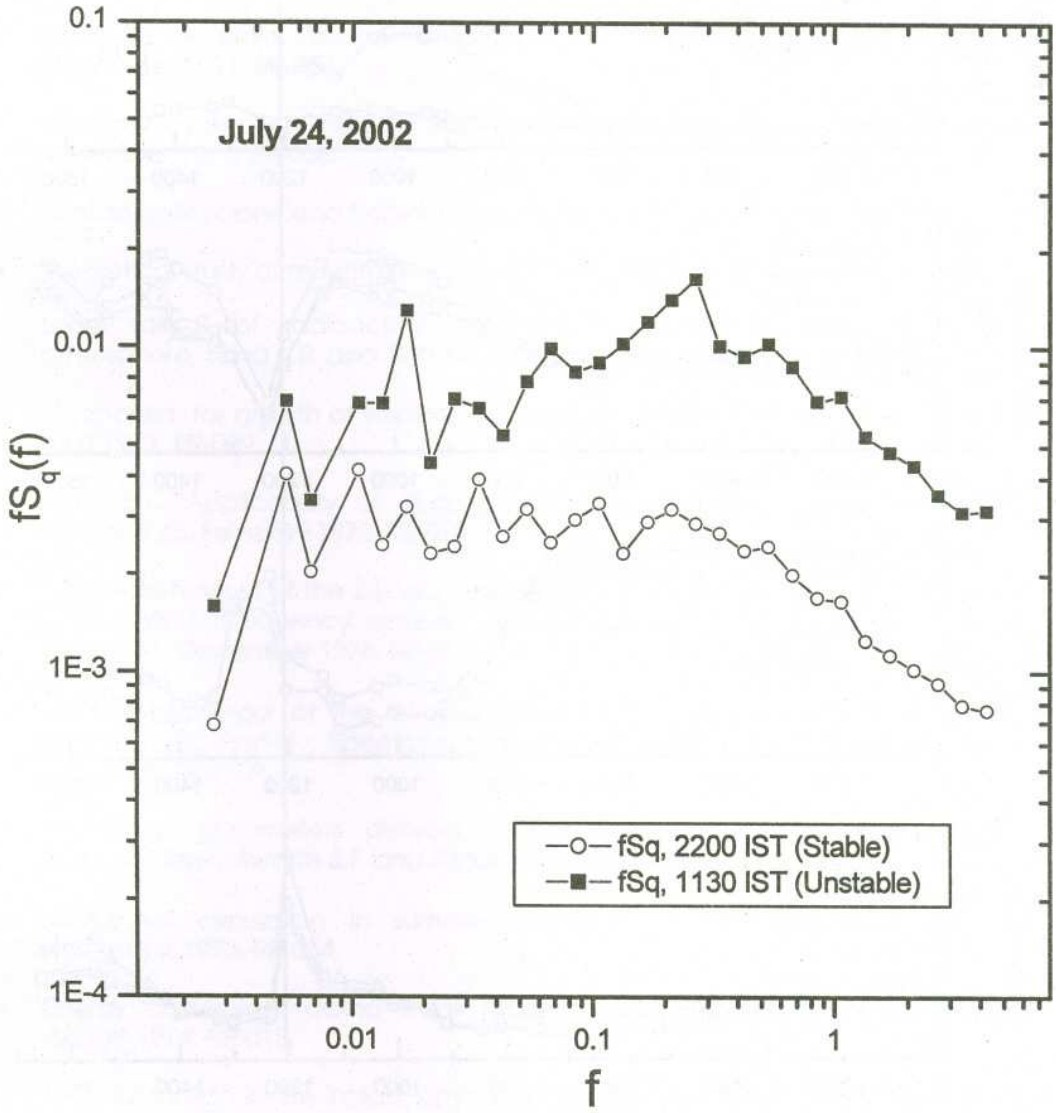

Fig.15 Spectra of water vapor for stable and unstable conditions

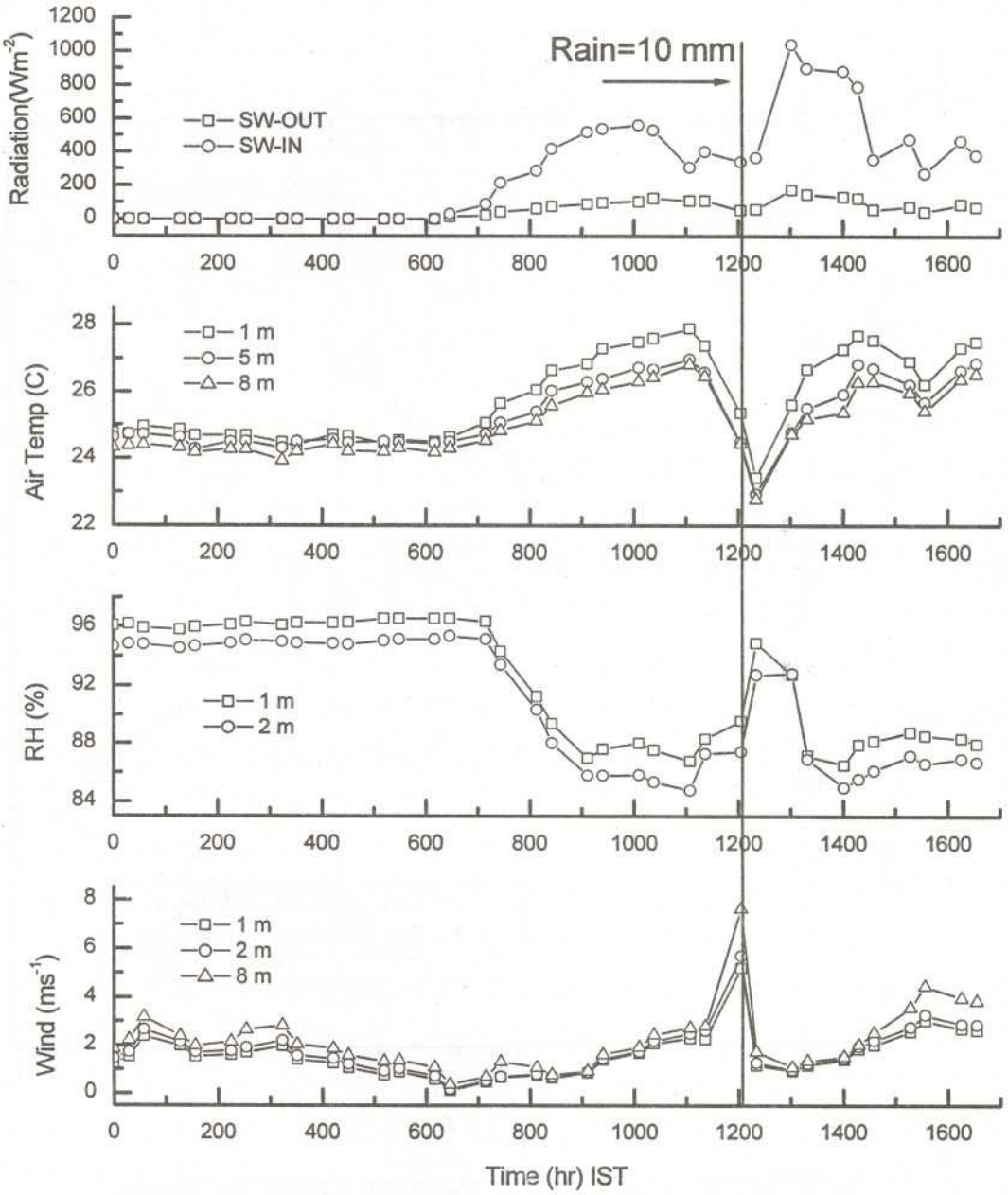

Fig.16 Response of meteorological parameters to precipitation (10 mm) on July 20, 2002.

I. I. T. M. RESEARCH REPORTS

- Energetic consistency of truncated models, *Asnani G.C.*, August 1971, RR-001.
- Note on the turbulent fluxes of heat and moisture in the boundary layer over the Arabian Sea, *Sinha S.*, August 1971, RR-002.
- Simulation of the spectral characteristics of the lower atmosphere by a simple electrical model and using it for prediction, *Sinha S.*, September 1971, RR-003.
- Study of potential evapo-transpiration over Andhra Pradesh, *Rakhecha P.R.*, September 1971, RR-004.
- Climatic cycles in India-1: Rainfall, *Jagannathan P. and Parthasarathy B.*, November 1971, RR-005.
- Tibetan anticyclone and tropical easterly jet, *Raghavan K.*, September 1972, RR-006.
- Theoretical study of mountain waves in Assam, *De U.S.*, February 1973, RR-007.
- Local fallout of radioactive debris from nuclear explosion in a monsoon atmosphere, *Saha K.R. and Sinha S.*, December 1972, RR-008.
- Mechanism for growth of tropical disturbances, *Asnani G.C. and Keshavamurty R.N.*, April 1973, RR-009.
- Note on "Applicability of quasi-geostrophic barotropic model in the tropics", *Asnani G.C.*, February 1973, RR-010.
- On the behaviour of the 24-hour pressure tendency oscillations on the surface of the earth, Part-I: Frequency analysis, Part-II: Spectrum analysis for tropical stations, *Misra B.M.*, December 1973, RR-011.
- On the behaviour of the 24 hour pressure tendency oscillations on the surface of the earth, Part-III : Spectrum analysis for the extra-tropical stations, *Misra B.M.*, July 1976, RR-011A.
- Dynamical parameters derived from analytical functions representing Indian monsoon flow, *Awade S.T. and Asnani G.C.*, November 1973, RR-012.
- Meridional circulation in summer monsoon of Southeast Asia, *Asnani G.C.*, November 1973, RR-014.
- Energy conversions during weak monsoon, *Keshavamurty R.N. and Awade S.T.*, August 1974, RR-015.
- Vertical motion in the Indian summer monsoon, *Awade S.T. and Keshavamurty R.N.*, August 1974, RR-016.
- Semi-annual pressure oscillation from sea level to 100mb in the northern hemisphere, *Asnani G.C. and Verma R.K.*, August 1974, RR-017.
- Suitable tables for application of gamma probability model to rainfall, *Mooley D.A.*, November 1974, RR-018.
- Annual and semi-annual thickness oscillation in thenorthern hemisphere, *Asnani G.C. and Verma R.K.*, January 1975, RR-020.

- Spherical harmonic analysis of the normal constant pressure charts in the northern hemisphere, *Awade S.T., Asnani G.C. and Keshavamurty R.N.*, May 1978, RR-021.

- Dynamical parameters derived from analytical function representing normal July zonal flow along 87.5 °E, *Awade S.T. and Asnani G.C.*, May 1978, RR-022.

- Study of trends and periodicities in the seasonal and annual rainfall of India, *Parthasarathy B. and Dhar O.N.*, July 1975, RR-023.

- Southern hemisphere influence on Indian rainfall, *Raghavan K., Paul D.K. and Upasani P.U.*, February 1976, RR-024.

- Climatic fluctuations over Indian region - Rainfall : A review, *Parthasarathy B. and Dhar O.N.*, May 1978, RR-025.

- Annual variation of meridional flux of sensible heat, *Verma R.K. and Asnani G.C.*, December 1978, RR-026.

- Poisson distribution and years of bad monsoon over India, *Mooley D.A and Parthasarathy B.*, April 1980, RR-027.

- On accelerating the FFT of Cooley and Tukey, *Mishra S.K.*, February 1981, RR-028.

- Wind tunnel for simulation studies of the atmospheric boundary layer, *Sivaramakrishnan S.*, February 1981, RR-029.

- Hundred years of Karnataka rainfall, *Parthasarathy B. and Mooley D.A.*, March 1981, RR-030.

- Study of the anomalous thermal and wind patterns during early summer season of 1979 over the Afro-Asian region in relation to the large-scale performance of the monsoon over India, *Verma R.K. and Sikka D.R.*, March 1981, RR-031.

- Some aspects of oceanic ITCZ and its disturbances during the onset and established phase of summer monsoon studied with Monex-79 data, *Sikka D.R., Paul D.K. and Singh S.V.*, March 1981, RR- 032.

- Modification of Palmer drought index, *Bhalme H.N. and Mooley D.A.*, March 1981, RR-033.

- Meteorological rocket payload for Menaka-II/Rohini 200 and its developmental details, *Vernekar K.G. and Brij Mohan*, April 1981, RR-034.

- Harmonic analysis of normal pentad rainfall of Indian stations, *Anathakrishnan R. and Pathan J.M.*, October 1981, RR-035.

- Pentad rainfall charts and space-time variations of rainfall over India and the adjoining areas, *Anathakrishnan R. and Pathan J.M.*, November 1981, RR-036.

- Dynamic effects of orography on the large scale motion of the atmosphere Part I : Zonal flow and elliptic barrier with maximum height of one km., *Bavadekar S.N. and Khaladkar R.M.*, January 1983, RR-037.

- Limited area five level primitive equation model, *Singh S.S.*, February 1983, RR-038.

- Developmental details of vortex and other aircraft thermometers, *Vernekar K.G., Brij Mohan and Srivastava S.*, November 1983, RR-039.

- Note on the preliminary results of integration of a five level P.E. model with westerly wind and low orography, *Bavadekar S.N., Khaladkar R.M., Bandyopadhyay A. and Seetaramayya P.*, November 1983, RR-040.

- Long-term variability of summer monsoon and climatic change, *Verma R.K., Subramaniam K. and Dugam S.S.*, December 1984, RR-041.

- Project report on multidimensional initialization for NWP models, *Sinha S.*, February 1989, RR-042.

- Numerical experiments with inclusion of orography in five level P.E. Model in pressure-coordinates for interhemispheric region, *Bavadekar S.N. and Khaladkar R.M.*, March 1989, RR-043.

- Application of a quasi-lagrangian regional model for monsoon prediction, *Singh S.S. and Bandyopadhyay A.*, July 1990, RR-044.

- High resolution UV-visible spectrometer for atmospheric studies, *Bose S., Trimbake H.N., Londhe A.L. and Jadhav D.B.*, January 1991, RR-045.

- Fortran-77algorithm for cubic spline interpolation for regular and irregular grids, *Tandon M.K.*, November 1991, RR-046.

- Fortran algorithm for 2-dimensional harmonic analysis, *Tandon M.K.*, November 1991, RR- 047.

- 500 hPa ridge and Indian summer monsoon rainfall : A detailed diagnostic study, *Krishna Kumar K., Rupa Kumar K. and Pant G.B.*, November 1991, RR-048.

- Documentation of the regional six level primitive equation model, *Singh S.S. and Vaidya S.S.*, February 1992, RR-049.

- Utilisation of magnetic tapes on ND-560 computer system, *Kripalani R.H. and Athale S.U.*, July 1992, RR-050.

- Spatial patterns of Indian summer monsoon rainfall for the period 1871-1990, *Kripalani R.H., Kulkarni A.A., Panchawagh N.V. and Singh S.V.*, August 1992, RR-051.

- FORTRAN algorithm for divergent and rotational wind fields, *Tandon M.K.*, November 1992, RR-052.

- Construction and analysis of all-India summer monsoon rainfall series for the longest instrumental period: 1813-1991, *Sontakke N.A., Pant G.B. and Singh N.*, October 1992, RR-053.

- Some aspects of solar radiation, *Tandon M.K.*, February 1993, RR-054.

- Design of a stepper motor driver circuit for use in the moving platform, *Dharmaraj T. and Vernekar K.G.*, July 1993, RR-055.

- Experimental set-up to estimate the heat budget near the land surface interface, *Vernekar K.G., Saxena S., Pillai J.S., Murthy B.S., Dharmaraj T. and Brij Mohan*, July 1993, RR-056.

- Identification of self-organized criticality in atmospheric total ozone variability, *Selvam A.M. and Radhamani M.*, July 1993, RR-057.

- Deterministic chaos and numerical weather prediction, *Selvam A.M.*, February 1994, RR-058.
- Evaluation of a limited area model forecasts, *Singh S.S., Vaidya S.S Bandyopadhyay A., Kulkarni A.A, Bawiskar S.M.,Sanjay J., Trivedi D.K. and Iyer U.*, October 1994, RR-059.
- Signatures of a universal spectrum for atmospheric interannual variability in COADS temperature time series, *Selvam A.M., Joshi R.R. and Vijayakumar R.*, October 1994, RR-060.
- Identification of self-organized criticality in the interannual veriability of global surface temperature, *Selvam A.M. and Radhamani M.*, October 1994, RR-061.
- Identification of a universal spectrum for nonlinear veriability of solar-geophysical parameters, *Selvam A.M., Kulkarni M.K., Pethkar J.S. and Vijayakumar R.*, October 1994, RR-062.
- Universal spectrum for fluxes of energetic charged particles from the earth's magnetosphere, *Selvam A.M. and Radhamani M.*, June 1995, RR-063.
- Estimation of nonlinear kinetic energy exchanges into individual triad interactions in the frequency domain by use of the cross-spectral technique, *Chakraborty D.R.*, August 1995, RR-064.
- Monthly and seasonal rainfall series for all-India homogeneous regions and meteorological subdivisions: 1871-1994, *Parthasarathy B., Munot A.A. and Kothawale D.R.*, August 1995, RR-065.
- Thermodynamics of the mixing processes in the atmospheric boundary layer over Pune during summer monsoon season, *Morwal S.B. and Parasnis S.S.*, March 1996, RR-066.
- Instrumental period rainfall series of the Indian region: A documentation, *Singh N. and Sontakke N.A.*, March 1996, RR-067.
- Some numerical experiments on roundoff-error growth in finite precision numerical computation, *Fadnavis S.*, May 1996, RR-068.
- Fractal nature of MONTBLEX time series data, *Selvam A.M. and Sapre V.V.*, May 1996, RR-069.
- Homogeneous regional summer monsoon rainfall over India: Interannual variability and teleconnections, *Parthasarathy B., Rupa Kumar K. and Munot A.A.*, May 1996, RR-070.
- Universal spectrum for sunspot number variability, *Selvam A.M. and Radhamani M.*, November 1996, RR-071.
- Development of simple reduced gravity ocean model for the study of upper north Indian ocean, *Behera S.K. and Salvekar P.S.*, November 1996, RR-072.
- Study of circadian rhythm and meteorological factors influencing acute myocardial infraction, *Selvam A.M., Sen D. and Mody S.M.S.*, April 1997, RR-073.
- Signatures of universal spectrum for atmospheric gravity waves in southern oscillation index time series, *Selvam A.M., Kulkarni M.K., Pethkar J.S. and Vijayakumar R.*, December 1997, RR-074.

- Some example of X-Y plots on Silicon Graphics, *Selvam A.M., Fadnavis S. and Gharge S.P.*, May 1998, RR-075.

- Simulation of monsoon transient disturbances in a GCM, *Ashok K., Soman M.K. and Satyan V.*,August 1998, RR-076.

- Universal spectrum for intraseasonal variability in TOGA temperature time series, *Selvam A.M., Radhamani M., Fadnavis S. and Tinmaker M.I.R.*, August 1998, RR-077.

- One dimensional model of atmospheric boundary layer, *Parasnis S.S., Kulkarni M.K., Arulraj S. and Vernekar K.G.*, February 1999, RR-078.

- Diagnostic model of the surface boundary layer - A new approach, *Sinha S.*, February 1999, RR-079.

- Computation of thermal properties of surface soil from energy balance equation using force - restore method, *Sinha S.*, February 1999, RR-080.

- Fractal nature of TOGA temperature time series, *Selvam A.M. and Sapre V.V.*, February 1999, RR-081.

- Evolution of convective boundary layer over the Deccan Plateau during summer monsoon, *Parasnis S.S.*, February 1999, RR-082.

- Self-organized criticality in daily incidence of acute myocardial infarction, *Selvam A.M., Sen D., and Mody S.M.S.*, Feburary 1999, RR-083.

- Monsoon simulation of 1991 and 1994 by GCM : Sensitivity to SST distribution, *Ashrit R.G., Mandke S.K. and Soman M.K.*, March 1999, RR-084.

- Numerical investigation on wind induced interannual variability of the north Indian Ocean SST, *Behera S.K., Salvekar P.S. and Ganer D.W.*, April 1999, RR-085.

- On step mountain eta model, *Mukhopadhyay P., Vaidya S.S., Sanjay J. and Singh S.S.*, October 1999, RR-086.

- Land surface processes experiment in the Sabarmati river basin: an overview and early results, *Vernekar K.G., Sinha S., Sadani L.K., Sivaramakrishnan S., Parasnis S.S., Brij Mohan, Saxena S., Dharamraj T., Pillai, J.S., Murthy B.S., Debaje, S.B., Patil, M.N. and Singh A.B.*, November 1999, RR-087.

- Reduction of AGCM systematic error by Artificial Neural Network: A new approach for dynamical seasonal prediction of Indian summer monsoon rainfall, *Sahai A.K. and Satyan V.*, December 2000, RR-088.

- Ensemble GCM simulations of the contrasting Indian summer monsoons of the 1987 and 1988, *Mujumdar M.* and *Krishnan R.*, February 2001, RR-089.

- Aerosol measurements using lidar and radiometers at Pune during INDOEX field phases, *Maheskumar R.S., Devara P.C.S., Raj P.E., Jaya Rao Y.,Pandithurai G., Dani K.K., Saha S.K., Sonbawne S.M. and Tiwari Y.K.*, December 2001, RR-090.

- Modelling studies of the 2000 Indian summer monsoon and extended analysis, *Krishnan R., Mujumdar M., Vaidya V., Ramesh K.V. and Satyan V.*, December 2001, RR-091.

- Intercomparison of Asian summer monsoon 1997 simulated by atmospheric general circulation models, *Mandke S.K., Ramesh K.V. and Satyan V.*, December 2001, RR-092.

- Prospects of prediction of Indian summer monsoon rainfall using global SST anomalies, *Sahai A.K, Grimm A.M., Satyan V. and Pant G.B.*, April 2002, RR-093.

- Estimation of nonlinear heat and momentum transfer in the frequency domain buy the use of frequency co-spectra and cross-bispectra, *Chakraborty D.R. and Biswas M.K.*, August 2002, RR-094

- Real time simulations of surface circulations by a simple ocean model, *P Rahul Chand Reddy, Salvekar P.S., Ganer D.W. and Deo A.A.*, January 2003, RR-095

- Evidence of twin gyres in the Indian ocean : new insights using reduced gravity model by daily winds, *P Rahul Chand Reddy, Salvekar P.S., Ganer D.W. and Deo A.A.*, February 2003, RR-096

- Dynamical seasonal prediction experiments of the Indian summer monsoon, *Milind Mujumdar, R. Krishnan and V. Satyan*, June 2003, RR-097

- Thermodynamics and dynamics of the upper ocean mixed layer in the central and eastern Arabian sea, *C. Gnanaseelan, A.K. Mishra, Bijoy Thompson and P.S. Salvekar*, August 2003, RR-098